KTH ROYAL INSTITUTE
OF TECHNOLOGY

Degree Project in applied electrochemistry

Second cycle 30 credits

Evaluation of real drive data of a refuse fuel cell truck

HAMPUS EURÉN

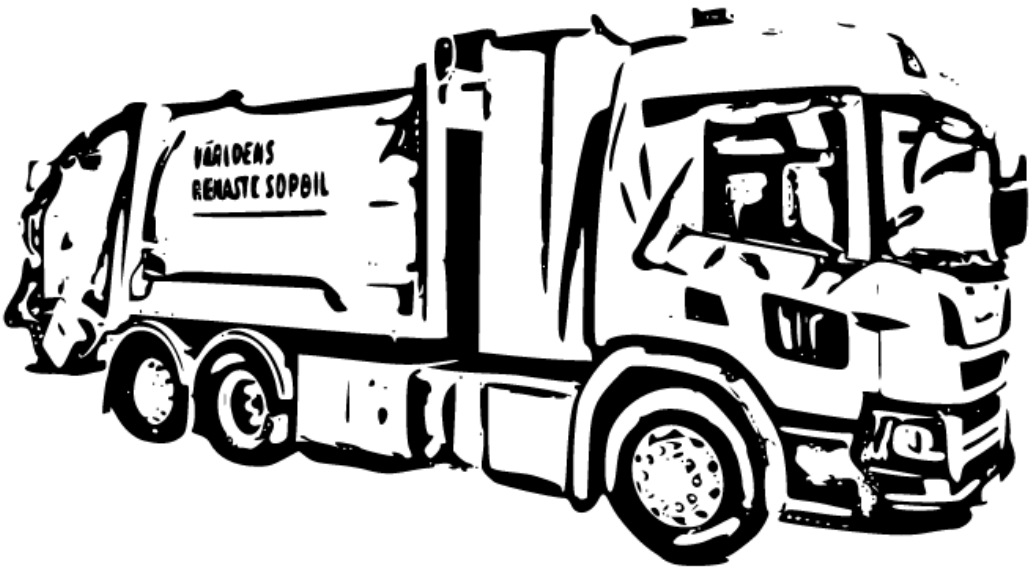

Stockholm, Sweden 2023

Author

Hampus Eurén, heuren@kth.se

M.Sc Chemical engineering for Energy and Environment

KTH Royal Institute of Technology

Stockholm, Sverige

Project location

Division of applied electrochemistry - KTH

Examiner

Prof. Göran Lindbergh,

KTH Royal Institute of Technology

Supervisors

Martina Butori,

KTH Royal Institute of Technology

Dr. Pontus Svens,

Scania

Abstract

Language: English

A consortium consisting of Scania, JOAB, Powercell Sweden AB, KTH, and Renova collaborated to design and engineer a fuel cell-powered refuse truck within a FFI-funded project. The refuse truck has been operational in Gothenburg since 2020, with a hydrogen gas infrastructure of one refuelling station at the time of this work. From 2020 to 2023, the fuel cell has gone through driving and standing still tests. Real drive data on the truck's system and fuel cell was recorded. The databases were unsynchronised in time, hence data synchronisation was required.

This thesis began with the main aim of developing an accelerated stress test for the fuel cell based on this application. Additionally, the aim was to evaluate the ageing of the fuel cell. Due to the available variables, fuel cell ageing was based on deterioration of fuel cell powers at constant temperatures and currents.

A test cycle (or power cycle) based on refuse truck test driving was developed instead. By utilising the established “k-means clustering” method on fuel cell power cycles, a test cycle representative of the truck operation from 2020 to 2023 was made. The test cycle was validated based on a statistical criterion, although verification and further work are required. After 141.80 hours of fuel cell power requests no ageing could be identified. More data from refuse truck operation is needed, also considering that an additional hydrogen refuelling station will be put in place in 2023 in Gothenburg, hence the drive pattern might vary. In this context, however, the results from this thesis lay the foundation for future research and offer an approach to study the fuel cell truck.

Keywords: Fuel cells, hydrogen, refuse truck, accelerated stress test, degradation

Language: Svenska
Ett konsortium bestående av Scania, JOAB, Powercell, KTH och Renova samarbetade för att designa och konstruera en bränslecellsdriven sopbil inom ett FFI-finansierade projekt. Sopbilen har sedan dess varit i drift i Göteborg från 2020 till 2023, med en vätgasinfrastruktur bestående av en tankstation vid tidpunkten för detta arbete. Under den tiden har bränslecellen genomgått kör- och stillastående tester. Verkliga kördata på sopbilens system och bränslecell registrerades. Databaserna var osynkroniserade i tid och därför krävdes datasynkronisering.

Detta examensarbete inleddes med huvudsyftet att utveckla ett accelererat åldringstest för bränslecellen baserat på denna applikation. Ett ytterligare syfte var att utvärdera bränslecellens åldrande. På grund av de tillgängliga variablerna baserades bränslecellens åldrande på försämring av elektrisk effekt vid konstanta temperaturer och strömmar.

En testcykel (eller effekt-cykel) baserad på testkörningen av sopbilen utvecklades istället. Genom att använda den etablerade metoden "k-means clustering" på bränslecellens effekt-cykler skapades en testcykel som var representativ för sopbils-körning från 2020 till 2023. Testcykeln validerades baserat på ett statistiskt kriterium, verifiering och ytterligare arbete krävs dock. Efter 141,80 timmars bränslecellsdrift kunde ingen åldring identifieras. Mer data från sopbilen behövs och faktumet att ytterligare en vätgastankstation kommer att installeras under 2023 i Göteborg innebär att sopbilens körmönster kan förändras. Resultaten från denna avhandling lägger dock grunden för framtida forskning och erbjuder ett tillvägagångssätt för att studera den bränslecellsdrivna sopbilen.

Keywords: Bränsleceller, vätgas, sopbil, accelererat åldringstest, åldring

Acknowledgements

No project ends up as you planned it in the beginning. When entering a project with a certain goal you have to be prepared to adapt it to the conditions of the project. When doing my thesis at the division of applied electrochemistry - KTH, I have learned a lot. Not only about both fuel cells and batteries but everything that orbit scientific work too. In that regard I wish to express my gratitude for the guidance and support that I have been handed; especially to my supervisor Martina Butori. Thank you for giving me the opportunity to work on this thesis.

To my family and all the friends, new and old. From you I can always learn something new from and enjoy your company. My time at KTH began and will continue with this. Cheers, Oskar.

Stockholm, June 2023

Hampus Eurén

Table of contents

Abbreviations

AMDT	Accelerated membrane durability test
AST	Accelerated stress test
BEV	Battery electric vehicle
BM	Binary method
BOL	Beginning of life
CAN	Central area network
CC	Cross correlation
CL	Catalyst layer
DOE	U.S. Department of Energy
DTW	Dynamic time warping
EMU	Electric motor unit
EU	European Union
FC	Fuel cell
HD	Heavy duty
HHV	Higher heating value
HOR	Hydrogen oxidation reaction
LHV	Lower heating value
LD	Light duty
LT	Low temperature
MEA	Membrane electrode assembly
NaN	Not a number
NEDC	New European Drive Cycle
OCV	Open circuit voltage
ORR	Oxygen reduction reaction
PEMFC	Polymer electrolyte membrane fuel cell
PEM	Polymer electrolyte membrane
SOC	State of charge
SST	Steady-state test
SD	Start-up
SU	Shut-down

1. Introduction

This chapter sets the stage for this thesis by introducing the background and purpose of this work, highlighting its significance in contributing towards national and global climate goals and future research. As denoted by the title, the focal point of this report revolves around the comprehensive evaluation of real drive data obtained from a refuse fuel cell truck. Delving into the complexity of the real drive data, this chapter also introduces the key research questions that will be addressed throughout the thesis.

1.1 Background

The European Union (EU) and its member states have the climate target of cutting greenhouse emissions by 40% until the year 2030. Some countries, such as Sweden, have the ambitious goal of cutting emissions from domestic transport by 70 % until the year 2045. [1] As of 2021, in Sweden 31 % of CO_2 emissions come from the transportation sector only. This includes both personal cars and e.g. industrial trucks. [2] To decarbonise the transportation sector, battery electric vehicles (BEVs) are regarded as a viable option for personal cars. In heavy-duty (HD) vehicle applications (trucks and buses) [3] one technology that is increasingly more researched is polymer electrolyte membrane fuel cells (PEMFCs). [3], [4]

A consortium consisting of Scania (the truck and bus manufacturer), JOAB (the truck body manufacturer), Powercell Sweden AB (the fuel cell developer), and Renova (the waste and recycling company) collaborated to design and engineer a fuel cell-powered refuse truck within the FFI-funded project. After several months of development, the truck was successfully built and has been operational in Gothenburg since 2020, although not in official service until April 2023. This innovative project aims to promote a sustainable and emissions-free transportation solution for heavy-duty vehicles. KTH is involved in the project, responsible for analysing real-world driving data. The refuse truck operates within the Gothenburg area. It is equipped with a powertrain consisting of a PEMFC-stack and a battery module. The truck, referred to as Albert, shown in Figure 1.1, weighs approximately 15 tonnes and carries 28 kg of hydrogen gas for fuel. The fuel cell serves as a supplementary power source, supporting the battery by charging it, supplying power to auxiliary devices, and assisting the electric-motor unit (EMU). Currently, the truck has been primarily driving within the Gothenburg region for drive testing; from April 2023 it is employed for the collection of cardboard in urban and extra-urban areas of the city.

Figure 1.1 A PEMFC refuse truck operational in Gothenburg refereed as Albert. [5]

The refuse truck is a pilot and has therefore gone through test-driving prior to April 2023. The focus of this thesis is the evaluation of real-drive data recorded between early 2020 until March 2023. The data processing was performed on MATLAB in the division of applied electrochemistry - KTH. This thesis studied FC ageing and developed a test cycle for PEMFCs based on the real-drive data. The work of this report served as a foundation for future studies on the project that involved the FC refuse truck.

Current research on PEMFCs primarily focuses on exploring novel materials that offer enhanced durability and reduced cost. Another area of interest is the development of test protocols and analytical tools that can simulate real-world scenarios of PEMFC operation. Researchers also aim to identify the most common causes of cell degradation and FC failure. [6], [7] The main obstacles to commercialising automotive PEMFCs lie in their cost and durability. The efficiency of PEMFCs during operation is influenced by various factors, including cell design, materials, and electrochemical and transport phenomena. Studies have demonstrated that PEMFC vehicles experience the highest degradation rates during startup/shutdown (SU/SD) and transient operation, which occur more frequently in transportation applications compared to stationary ones. [8], [9] Therefore, there is a need for efficient testing methods for FCs that save time and materials in the transportation sector. This is essential to show that FCs are a viable technology in the transition to electrification of transportation.

The reasons why research on PEMFCs for HD vehicle applications has increased are due to the benefits that the technology can provide. In Sweden, drivers of trucks in service are typically allowed a maximum drive time of 9 hours per day. [10] During this time, a significant portion is often spent on highways. Consequently, trucks require a substantial energy storage system capable of providing sufficient range for long-distance missions. FCs in general have higher specific energy than batteries. [8], [11] For HD BEVs to achieve the same mileage, increased battery size, hence BEV weight, becomes a necessity. This results in reduced freight capacity and higher energy consumption for propulsion.

Although not yet at a commercial scale, HD vehicle applications based on PEMFCs have been proven to be a viable solution and some pilot examples have been demonstrated. One notable research paper on PEMFCs for HD vehicles involved bus application. In Whistler Resort Community, 20 FC buses with a Ballard HD6 Module were deployed in 2010. Real-drive data was collected to develop an Accelerated Membrane Durability Test (AMDT) protocol for PEMFC vehicles. The AMDT reduced testing time and achieved successful results. [12] Another study, conducted in Taiwan, examined the performance of FC hybrid-drive electric forklifts. The vehicles used a PEMFC with auxiliary power modules (lithium ion battery and super capacitor) for driving and lifting. Real drive data showed power segregation linked to operator habits. [13] An ongoing initiative supported by the EU is the Revive project, which commenced in 2018 and is scheduled to conclude in 2024. The primary objective of this project is to design, evaluate, and field-test several FC refuse trucks in urban environments. [14] The subsequent section summarises the real drive data and interviews conducted.

1.2 The real drive data

The powertrain of the refuse truck, that this thesis covers, consists of a LT-PEMFC stack and a battery module. The LT-PEMFC can deliver a gross maximum power of 80 kW. Real-drive data was collected with two separate loggers. One logger records the FC data, and the other one records the system part of the truck i.e. signals on the central area network (CAN). The CAN includes the traction battery data. Data recording begins once the truck ignition is activated (i.e. the keys are inserted in the truck and the system is switched on).

The logged data consist of many system variables which are not of interest for this work. However, the variables of interest involve electrochemical data from both the LT-PEMFC and battery (e.g. current, voltage and state of charge (SOC)); and refuse truck data (e.g. vehicle speed, mass and geo-coordinates).

The FC refuse truck this thesis works with is a pilot. Thus, the usage pattern of the truck has changed with time. This was observed in the data. In addition to this, most of this consists of test driving between sites and few actual testing of the PEMFC. The desired data for this thesis were the ones where the truck was operational. Some files were therefore disregarded. Other signs of usefulness were if variable(s) of interest did not contain corrupted data, e.g. undefinable not a number-points (labelled NaN in the data vectors).

In addition to the loggers, two interviews were held with Renova representatives on separate occasions, 2023-01-26 and 2023-05-02 respectively. The first involved the person responsible for the project at Renova and the second the person which usually operates the truck. In the first interview it was revealed that the refuelling station was out of service almost the entire 2022, with some exceptions. The interviewee also informed that parking, safety (in case of accidents) and refuelling protocols for Hydrogen trucks were not established at the time of the interview. Plans for establishing a second refuelling station close to Renova facility in 2023 are in motion.

The second interviewee, the only driver of the truck at that time, told about the impressions he had about the refuse truck after operating it in April 2023 in relation to the new technology used. The driver was positive about the refuse truck, emphasising that the truck is quiet when comparing it with internal combustion engine refuse trucks. However, he thought that he still had to get used to learning how to drive efficiently to minimise Hydrogen fuel consumption.

However, after that there were hardly any issues with the truck, unless they were due to the refuelling station.

1.3 Research questions

The refuse FC truck, referred to as Albert, driving in Gothenburg is a pilot study. This master thesis is therefore conducting research on this case study. Due to limitations in Hydrogen gas refuel infrastructure in Gothenburg and the Covid-19 pandemic, the testing of the refuse FC truck has in some periods been delayed. In spite of this, exploring the potential of the test truck, evaluation of the usage pattern and the FC durability in this application were points of interest. To contribute to HD PEMFCs studies, lay groundwork for future work and analysis of the refuse truck application, the following research questions were considered in this thesis.

1. *Development of a test cycle that ought to represent a typical single day driving pattern followed by the truck.*
2. *Quantification and, if possible, forecasting of degradation/ageing of the fuel cell performance in this pilot truck.*

1.4 Thesis outline

The next chapters in this thesis will cover the following: Chapter 2 lays foundation for the test cycle development i.e. the basics of the FC and what causes failure mechanisms. In addition, examples of accelerated stress tests and their load cycles are included for reference. Chapter 3 explains the methodology: the steps taken to reach the aims of the research questions. In Chapter 4 are the main results introduced. Comments and discussions on the main results and the work of this report are in chapter 5. The report closes up with a remarks and conclusions section in Chapter 6.

2 PEMFCs basics

A PEMFC in essence converts the chemical energy of Hydrogen and Oxygen into electrical work, producing water as a product and heat as a by-product. The theoretical maximum work and heat output based on the reversible cell voltage can be determined through the fundamental principles of chemistry and thermodynamics. [15]

2.1 Electrochemical thermodynamics

The chemical process of a PEMFC involves Hydrogen gas being supplied to the anode, where Hydrogen oxidation reaction (HOR) takes place, while simultaneously Oxygen reduction reaction (ORR) occurs at the cathode. HOR is depicted in reaction (I), ORR in reaction (II) and the full cell reaction of the fuel cell is depicted in reaction(III).

Anode: $H_2 \rightarrow 2H^+ + 2e^-$ **(I)**

Cathode: $½O_2 + 2H^+ + 2e^- \rightarrow H_2O$ **(II)**

Full cell: $½O_2 + H_2 \rightarrow H_2O(l)$ **(III)**

By utilising the stoichiometry and specific heat of formation of the reactants and product in reaction (III), the thermodynamic properties listed in Table 2.1 can be derived. These properties, presented under standard conditions (p = 1 atm, T = 298.15 K), vary with temperature and pressure. Higher temperatures lead to increased specific enthalpy and entropy. In this example does the properties belong to the higher heating values (HHV) of (III). [15]

Table 2.1. The standard* specific enthalpy, entropy and free energy from reaction (III).

	Specific enthalpy, ΔH [kJ/mol]	Specific entropy, ΔS [kJ/K.mol]	Specific Gibbs free energy, ΔG=ΔH-TΔS [kJ/mol]
H_2O (l)	-285.8	-0.163	-237.2

*Standards conditions p = 1 atm, T = 298.15 K [15]

Table 2.1 shows that the water formation reaction in reaction (III) releases heat (exothermic) and results in a decrease in gas entropy (ΔS). Simultaneously, the surroundings experience an increase in entropy due to the released heat, which is given by TΔS. The total electrical work that a PEMFC can generate, represented by the Gibbs free energy of the cell (ΔG), is proportional to the standard cell potential (E^o_{Cell} [V]) as described by equation (IV).

$$E^{\circ}_{Cell} = \frac{-\Delta G}{nF} \quad \textbf{(IV)}$$

n represents the number of electrons involved in the redox reaction (in this case, n=2), and F = 96 485 [C/mol] represents Faraday's constant. Under standard conditions, the maximum theoretical cell voltage of a PEMFC is $E°_{Cell}$ = 1.229 V. The theoretical or thermodynamic efficiency, η_T, can be defined using equation (V).

$$\eta_T = \frac{"Available\ work"}{"Total\ energy\ in\ the\ system"} = \frac{\Delta G}{\Delta H} \quad \textbf{(V)}$$

In the same standard conditions, the theoretical maximum efficiency is η_T = 83 %. The cell potential in an ideal PEMFC is determined by various physical factors, which can be described by the Nernst equation (VI) for the Hydrogen/Oxygen FC.

$$E_{Ideal\ Cell} = E^{o}_{Cell}(T) + \frac{RT}{nF} ln\left(\frac{P_{H_2} \cdot P_{O_2}^{0.5}}{P_{H_2O}}\right) \quad \textbf{(VI)}$$

The Nernst equation demonstrates how the cell voltage of a PEMFC is influenced by factors such as the partial pressures of reactants and product, temperature (T [K]), and partial pressure (P [bar]). [15] The Nernst equation (VI) is important because the FCs run on the anode and cathode pressures i.e. higher pressures result in higher voltage meaning more power is produced.

2.2 Dynamic conditions

Under dynamic conditions, electrochemical phenomena cause deviations from ideal behaviour in the cell. Voltage losses occur due to activation, ohmic, and concentration polarisation effects at current density levels low, medium and high. Figure 2.1, the polarisation curve, depicts the relationship between cell voltage, current density, power density, and efficiency. The black line in the figure is the cell voltage. Low current densities between 0.0 and 0.2 A/cm^2 is the activation region i.e. an activation energy of the HOR and ORR is needed to start the reactions. Medium current densities between 0.2 and 1.2 A/cm^2 is the ohmic region (linear part of the voltage curve). The linear voltage drop is caused by the resistance of the conduction of ions in the polymer electrolyte membrane (PEM). High current densities between 1.2 and 1.5 A/cm^2 is the concentration region. The reactant gases are consumed in such a rate that concentration gradients appear i.e. lower reactant gas partial pressures at the electrodes. As described by equation (VI), the cell voltage decreases at lower gas pressures. [16]-[18]

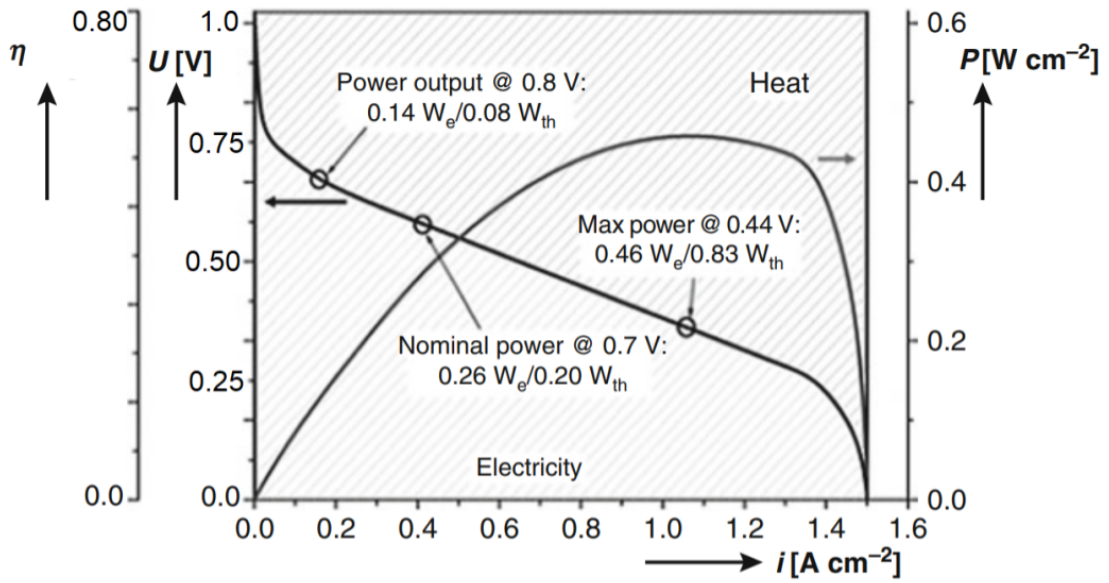

Figure 2.1 Cell voltage, voltage efficiency and Power density vs. current density. Black line: cell voltage U; grey line: power density. Picture is modified from. [8]

Figure 2.1 provides insights into the impact of loss phenomena on cell performance. Higher current densities result in lower power densities and efficiencies. [16]-[18] The efficiency depicted in the figure 2.1, known as voltage efficiency (η), measures the deviation of the cell voltage from the reversible open circuit voltage (OCV) (in this case, $E°_{Cell}$ = 1.229 V). It can be calculated using equation (VII).

$$\eta = \frac{E_{Cell}}{E_{Ideal\ Cell}} = \frac{E_{Cell}}{1.229} \qquad \textbf{(VII)}$$

2.3 Components & properties

The components and their properties have to be carefully chosen, designed and manufactured in PEMFCs. A simple depiction of a single PEMFC is illustrated in Figure 2.2. The figure shows also the reactant/product schematic. When LT-PEMFCs operate as in Figure 2.2, typically a temperature range of 60-80℃ is used for operation. The PEMFC in the figure is constructed by the components: BP = Bipolar plate; G = Gasket; GDL = Gas diffusion layer; CL = Catalyst layer; PEM = Polymer electrolyte membrane.

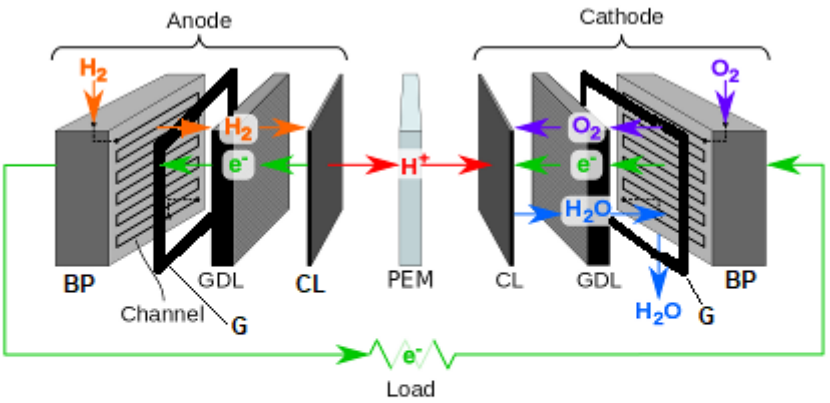

Figure 2.2 The construction of a PEMFC and the gas reactant schematic. Picture is modified from [19].

The schematic in Figure 2.2 can be explained as follows: Hydrogen gas is transported through the BP, GDL and reaches the CL (anode side) where reaction (I) (HOR) occurs. While the electrons are transported through the external circuit at which the load to be powered is connected, the Hydrogen cations are then transported through the PEM towards the CL (cathode). Similarly, Oxygen gas is transported to the CL (cathode side) where reaction (I) (ORR) occurs. The CL and the PEM make up for what is called the membrane electrode assembly (MEA), which is the heart of the PEMFC. [20] The MEA components functions and properties are summarised in Table 2.1.

Table 2.1 The main components in a PEMFC and their desired properties. [6], [17]

Component	Function	Material	Properties
CL	Speed up HOR and ORR. transportation of protons and reactants.	Pt or Pt-alloy nanoparticles on carbon support with an ionomer.	Catalytic surface area uniformity Porosity. Protonic conductivity.
PEM	Transportation of protons. Electric insulator. Hinder gas to cross through.	Perfluorosulfonic acid e.g. Nafion. [20]	Low electric conductivity. Good protonic conductivity. Electrochemical inertness. Gas non-permeability.

PEMFCs have significant potential for applications like portable energy storage and autonomous systems, with a thermodynamic efficiency of up to $\eta_{T,\ HHV}$ = 83 %. The lower heating value (LHV) (water gas product instead of liquid) theoretical efficiency is $\eta_{T,LHV}$ = 94.5 %. [6], [15] However, real-world PEMFCs exhibit voltage efficiencies ranging from 40-60 % (LHV). [21] The efficiency and ageing of PEMFCs can be negatively impacted by chemical and physical changes, making durability a key area of research. [8]

2.4 Research on PEMFCs

The non-ideality of the PEMFC components are due to unwanted processes occurring, efficiency of component functions and degradation of component properties. The unwanted processes include both transport and (electro)chemical phenomena. FC tests today aim at replicating conditions which happen in real applications, such as real-driving conditions. To achieve proper representability of the FC application, understanding of the conditions and mechanisms that lead to FC failure is imperative.

2.4.1 Stressors & degradation mechanisms

The CL and PEM are the key components that significantly impact the efficiency of a PEMFC. Under various operating conditions, temporary or permanent efficiency losses can occur within a PEMFC. These efficiency losses are due to multiple stressors which are summarised in Figure 2.3.

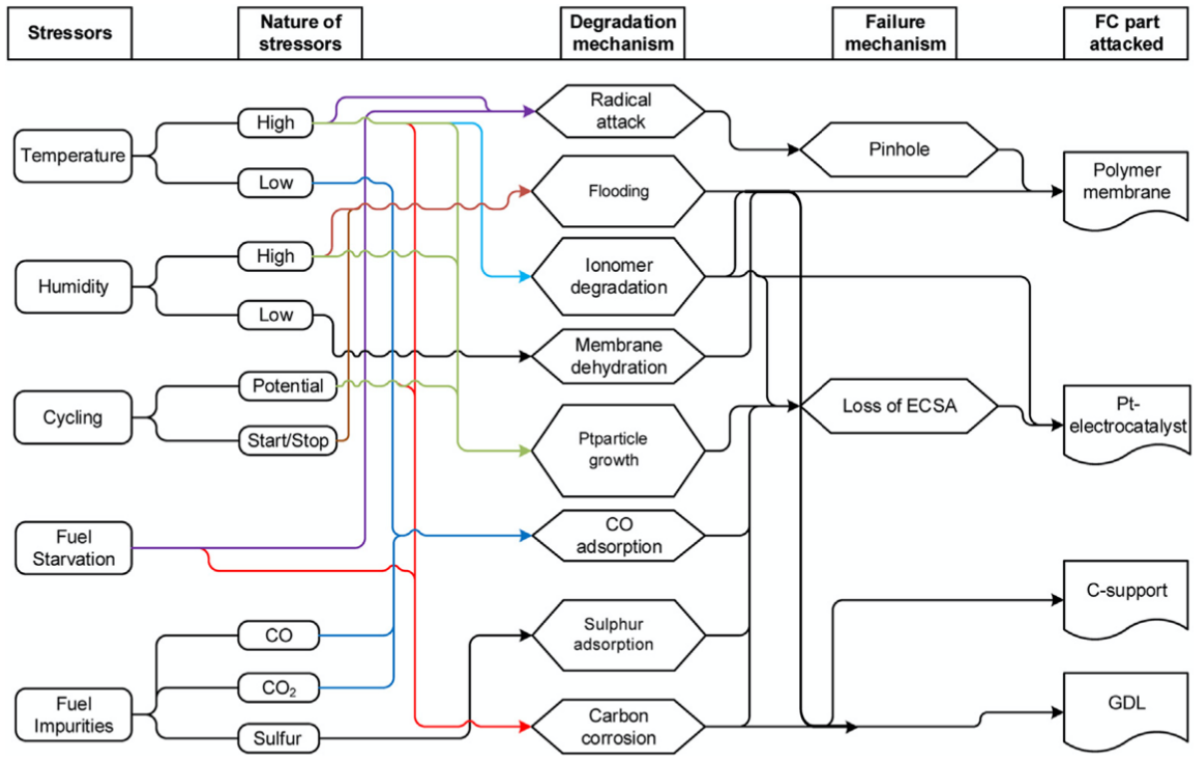

Figure 2.3 Summary of PEMFC stressors and degradation mechanisms. ECSA = Electrode Catalyst Surface Area; C-support = Carbon-support. [18, p. 09]

Stressors in a PEMFC can result in chemical, thermal, and mechanical degradation. Chemical degradation occurs due to radical attacks, leading to a loss in proton conductivity within the PEM. Thermal degradation can occur at temperatures above 80 °C and freezing temperatures, negatively impacting ionic conductivity and increasing gas permeability. [22] Mechanical

degradation may arise from manufacturing defects and varying levels of relative humidity within the PEM. [3], [23]

Specific stressors, such as Start/Stop events (SU/SD), induce changes in the cathode potential, causing the reverse reaction of Hydrogen oxidation and Oxygen reduction to occur, along with temporary gas starvation. These conditions, coupled with high potentials, contribute to Pt-catalyst degradation and carbon corrosion within the PEMFC. [24], [25] Consequently, these stressors cause irreversible efficiency loss and accelerate degradation.

The expected lifetime of stationary PEMFC applications is 30 000 hours, while for personal cars, it is around 5,000 hours (when the PEMFC is the primary power source). [26] Dynamic load conditions, such as urban driving, involve frequent acceleration and braking, unlike stationary applications where the load remains relatively constant over time. [18] PEMFCs in PEMFC and battery systems in HD vehicle applications have shown to exceed 25 000 hours of system lifetime. [27] The PEMFC aids the battery by charging it, thus minimising stress conditions such as voltage cycling.

2.4.2 Testing protocols for mimicking of real-life operations

Two methods commonly used for evaluating FC durability are steady-state tests (SST) and accelerated stress tests (AST). However, SSTs are often considered impractical due to their lengthy duration and high costs. For instance, conducting an SST on PEMFCs in a light-duty (LD) vehicle would require approximately 5000 hours of testing, involving daily hours of operation to simulate real driving conditions. Additionally, the use of Hydrogen in such tests adds to the expenses. ASTs on the other hand, typically last between 70 and 1000 hours. ASTs offer a more practical approach, particularly for testing the durability of PEMFC vehicles.[28]

To replicate realistic usage patterns, researchers design AST protocols based on real-world driving data. While a single AST protocol may not cover all aspects comprehensively, it aims to investigate the effects of specific stressors encountered in real-life environments where PEMFC vehicles operate. [7] Especially in vehicle applications, dynamic cycling stressors result in the greatest degradation of PEMFCs. [28]

Several examples of test protocols exist, including the PEMFC durability test protocol developed by the U.S. Department of Energy (DOE) in 2007 (Figure 2.4) [7][29], the New European Drive Cycle (NEDC) introduced in 2016 (Figure 2.5) [30], and protocols developed as part of the ID-fast project, concluded in 2021 (Figure 2.6). [31]

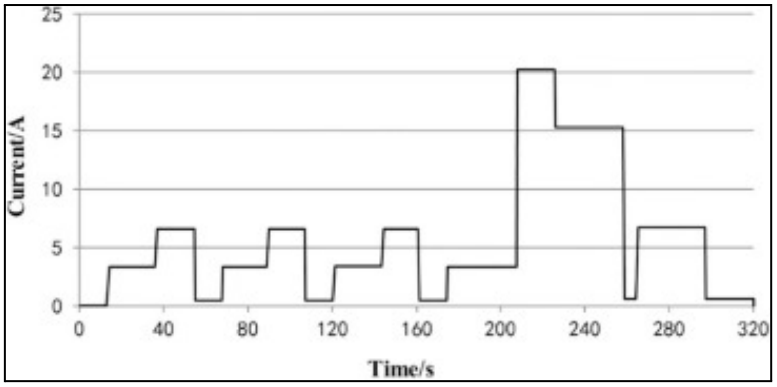

Figure 2.4 The DOE PEMFC durability DST protocol. [7]

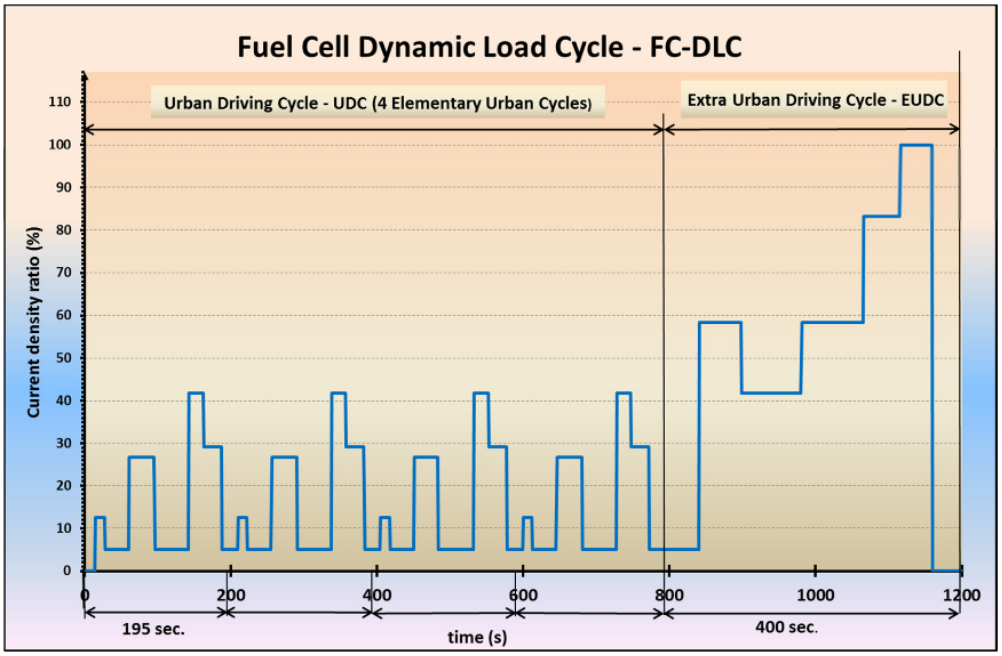

Figure 2.5 NEDC fuel cell dynamic load cycle. [30]

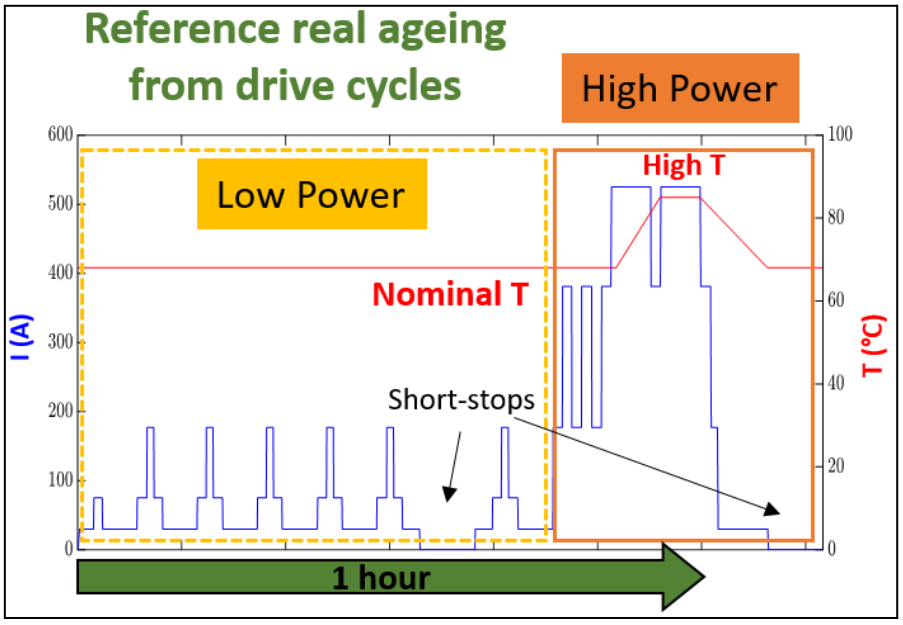

Figure 2.6 Protocols developed for accelerated stress tests by ID-FAST. [32]

The AST examples are all developed for LD PEMFC vehicles. As illustrated in Figures 2.4-2.6, AST protocols contain different amounts of repeated urban drive cycles. What also differentiates them is what traffic environment they represent, thus the duration of each drive cycle. However, each exhibits low and high load sections in the protocols. The more modern ASTs include more SU/SD cycles as seen in Figures 2.5 and 2.6. The real duration of ASTs are not highlighted in the figures, these are but the drive cycles that are to be repeated some amount of time.

3. Methodology

In this work a test cycle representative of a FC refuse truck's typical day of operation is developed. Additionally, the evaluation of any degradation to the FC performance is carried out using both a qualitative and quantitative approach. The methodology begins with describing the data processing and the data filtration employed on the refuse truck data.

3.1 Data processing

In the beginning two large sets of data were provided by PowerCell (FC-set) and Scania (S-set), respectively. Due to the quality of the data, a large portion of files were not used for the first research question in its initial formulation. The FC-set comprises 727 files, while the S-set consists of 1416 folders containing multiple files. The variables of interest in the S-set include battery and user display data, among others. For a comprehensive overview of the variables from both sets, see Table 3.1.

The two datasets consisted of different recording lengths and dates. Therefore, a synchronisation was required. Moreover, the two loggers were recorded using different frequencies, hence the FC data had to be down-sampled to 10 Hz. However, the synchronisation revealed that there were only a few times when the truck was doing refuse truck service work. This was identified by examining the truck's geographical coordinates in the synchronised files, which revealed that the truck primarily travelled between PowerCell and Scania facilities in Gothenburg, probably for some driving tests. Since the vehicle weight data was not reliable, see Appendix A1, and the FC power profile showed a variety of characteristics, no indication of recurring refuse material collection or refuse truck duties/usage patterns could be detected.

Table 3.1 The variables of interest from the FC- and S-dataset.

FC-set		**S-set***	
Time	[UTC]**	Time	[UTC]
FC stack current***	[A]	Battery current	[A]
FC stack voltage	[V]	Battery State of charge	[%]
FC cell average voltage	[V]	Battery voltage	[V]
Pressure, H_2, in	[barG]	Vehicle speed	[km/h]
Pressure, air, in	[barG]	Longitude	[degrees]
Pressure, coolant, in	[barG]	Latitude	[degrees]
Temperature, air, in	[°C]	Altitude	[degrees]
Temperature, coolant, in	[°C]	Vehicle mass	[tonnes]
Temperature, coolant, out	[°C]	H_2 amount in the tank (H_2%)	[%]

*The S-set contains many more signals, these were the ones useful for the goal of this study; **UTC = Universal time clock; *** Gross.

The variables of interest shown in Table 3.1 are the data series that this thesis was limited to. The thesis focused on the FC part of the truck. For this reason, the S-set served merely as an indicator of what the truck was doing; contextualising the FC load requirement in relation to the truck duty. Additionally, the stack temperature of the FC was assumed to be homogeneous although it was not provided in the logger. As a temperature reference, the average of the coolant temperatures (T_{Av}) in Table 3.1. was used to compare polarisation curves recorded at different FC temperatures in order to quantify any FC ageing (research question 2).

The data was processed using MATLAB. The variable nature of the data, explained in section 1.2, was explored during the data treatment. As a result, it became necessary to filter the datasets in order to extract the relevant data for addressing research question 1. The data processing attempt of all the files was set out to be automated, analysing one FC set file at the time. The variance of the data was dependent on when it was recorded: new attributes of the files appeared later on the timeline of the data recordings.

Many FC-sets contained data recorded by the logger while the FC was completely inactive. To extract the files where the FC was delivering power when the truck was in service filters were applied, basing the filtration on the FC stack gross power, P [kW]. This was calculated

with equation (VIII). The filtration of the FC set is summarised in the domain chart in Figure 3.1.

$$P = E_{Stack} \cdot I_{Stack} \quad \textbf{(VIII)}$$

Where E_{Stack} [V] is the stack voltage and I_{Stack} [A] is the stack current. If the FC delivered nearly zero power throughout the file i.e. P(max) = 0, the file was not included for the analysis. P(max) = 0 is represented as the blue domain in Figure 3.1 while P(max) > 0 the magenta coloured domain.

When looking into FC files manually, PEMFC corrupted recordings were discovered. These exhibited cell average voltages that were either negative or above OCV (i.e. approximately 1 V). These were not of use for either research question, hence they were removed because they were deemed unhelpful. The theoretical number of cells in the PEMFC stack served as an indicator of usefulness. The number of cells, N [-], can be calculated with equation (IX).

$$N = E_{Stack}/E_{Cell} \quad \textbf{(IX)}$$

E_{Cell} [V] is the average cell voltage. If N is beyond the real number of cells, 455, with a tolerance of 5 i.e. N ≠ (450 460) then the FC-file was considered potentially not useful and analysed manually. Verification of this is presented in Appendix A2. If any of the FC temperatures in Table 3.1 and the coolant average temperature are outside the range of LT-PEMFC operating temperature i.e. T ≠ [40 80]℃ at P(max), then the files are saved for later investigation. This is because they were considered a file of potentially FC testing (Figure 3.1 yellow domain). The FC files of use are represented by light blue in Figure 3.1.

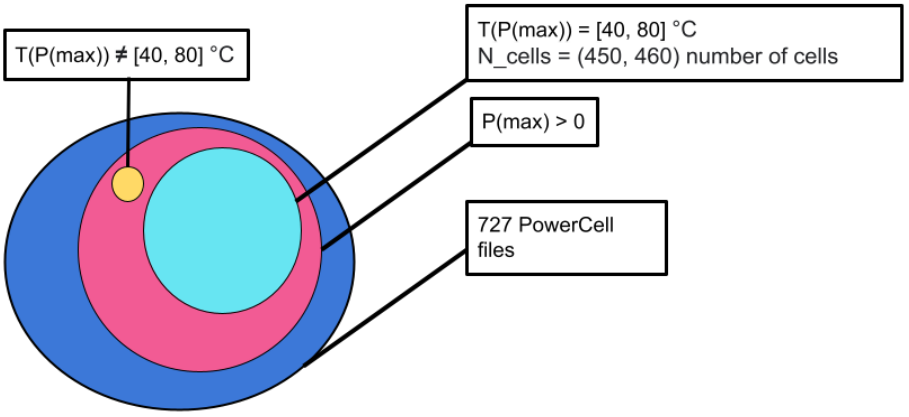

Figure 3.1 A domain chart representing the FC set and the subsets created from the data filtration.

For what concerns the S-set, the vehicle mass signal was deemed to lack accuracy and precision, see Appendix A1. Hence, collection and compressing of refuse material could not be deduced in the data. Also, first recording of the vehicle mass began from 2021-06-11. The time of FC and S-set recordings did not begin or end at the same time, the time difference was not constant between the sets. The H_2 % signal did not appear in the data until recordings from 2021-10-12 and onwards.

Also the S-set required filtration, as summarised by the domain chart in Figure 3.2. The duration of the recorded files varied ranging from less than 1 minute to over 1 hour and the S-set files which shared dates with the FC set were but a portion (red domain in Figure 3.2). The extraction of the synchronisation signals were automated. The battery power (P), SOC, vehicle speed, and FC power was considered useful for performing the synchronisation and verifying it. However, signals could be empty or corrupted (values of zero or NaNs in vectors) in some files and was deemed un-useful. These are depicted SOC = {} and P = {} in Figure 3.2. SOC and P signals which were of no use are represented by yellow and blue respectively in Figure 3.2.

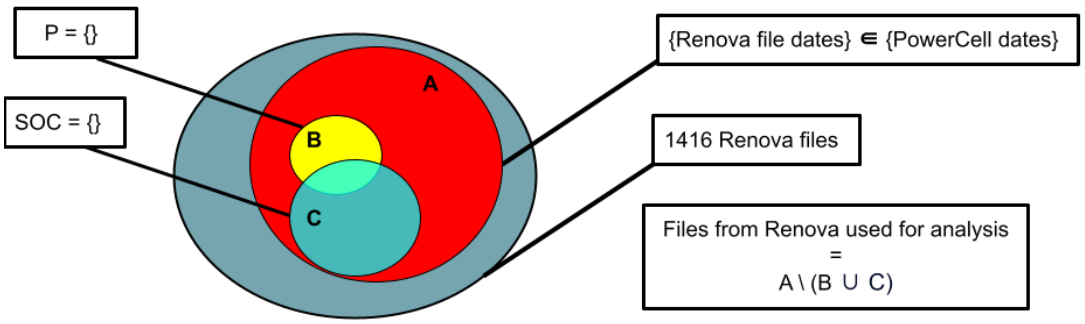

Figure 3.2. A domain chart representing the S set and the subsets created from the data filtration.

The synchronisation development was finalised as an iterative process; discrepancies had to be discovered. The subsequent section describes the synchronisation procedure.

3.2 Synchronisation

When constructing the programme for the synchronisation, errors and irregularities had to be detected before optimisations could be made. To save computational time, files from the FC-set were down-sampled from 100 Hz to 10 Hz using the MATLAB "downsample" function. [33]

Because H_2% signals appeared later in the files, to utilise files recorded prior to the availability of H_2%, FC and battery power are used for synchronisation. SOC and vehicle speed data are used for verifying the synchronisation. The synchronisation process is explained using one example of FC data shown in Figure 3.3. Additional examples of synchronisation can be seen in Appendix A3.

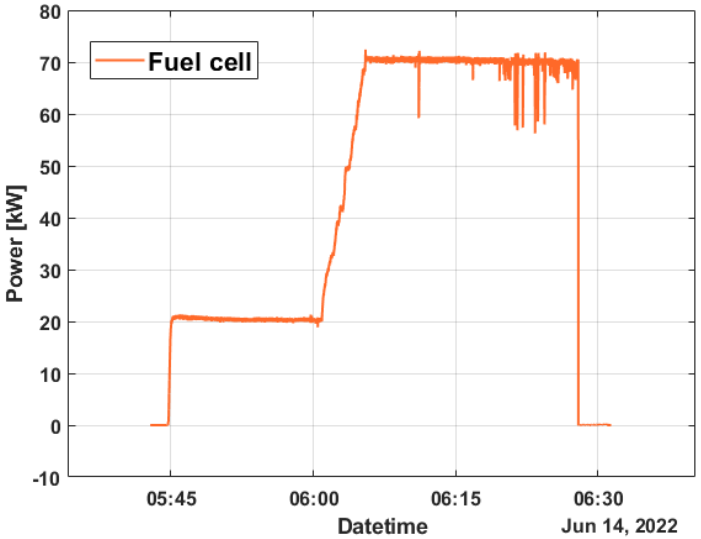

Figure 3.3 FC power cycle, used as example file for the synchronisation.

Two synchronisation methods were explored: dynamic time warping (DTW) [34] and cross correlation (CC). [35], [36] However, neither method gave results that were satisfactory for this work. Figure 3.4 illustrates the FC power in comparison to battery power, highlighting the dynamic behaviour of the battery. Although other instances of FC operation displayed dynamic behaviour (see Appendix A1-A4), the DTW and CC methods encountered difficulties in handling such diverse datasets.

Owing to these challenges, a third method, designed for this particular work, was employed (called the binary method (BM)) in this work. The method in essence transforms the FC and battery power into binary sets and shifts the battery data in time if a criterion is met in that time position. The fixed or reference time is thus the FC datetime. The transformed version of Figure 3.4 can be observed in Figure 3.5.

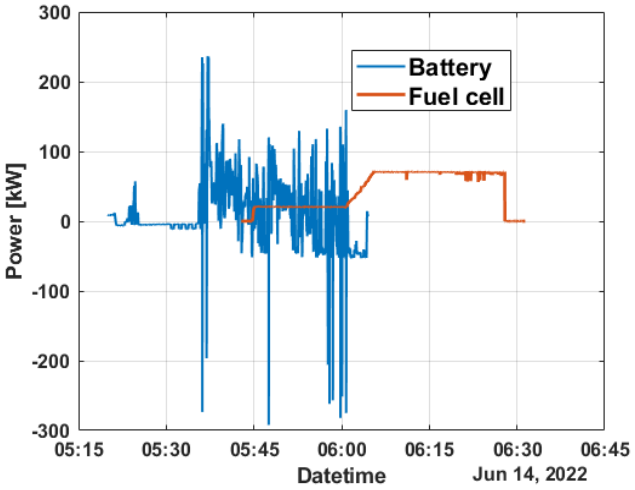

Figure 3.4 FC and battery power versus time.

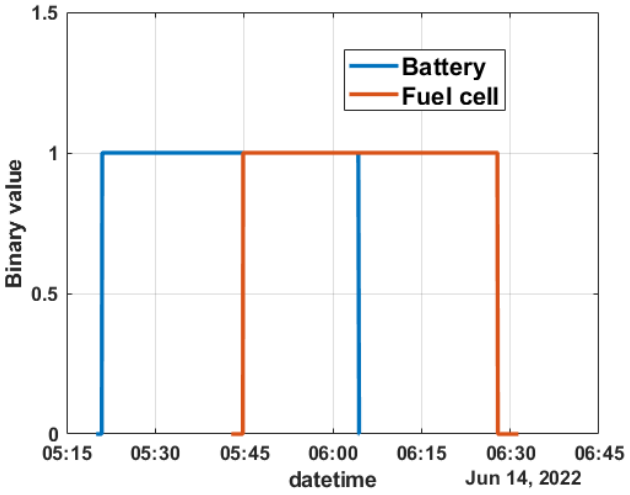

Figure 3.5 Binary sets of the data in Figure 3.4.

The bins represent time intervals of operation above a fixed or adjustable power output threshold. Through an iterative process, the final criteria for the FC-set was established: if the absolute value of FC power exceeded 10 kW, the binary set element was assigned a value of 1; otherwise, it was set to 0 (Figure 3.5.). For the S-set, an adjustable criterion was required due to the transient nature of the battery power profiles. If the absolute value of the battery power exceeded the average battery power, the binary set element was assigned a value of 1; otherwise, it was set to 0. In some cases, adding a constant value, such as 0.05 kW, to the criteria improved the precision of the transformation and synchronisation.

After the binary sets are made, as shown in Figure 3.5, the bins with similar properties are identified. The last position in time of the battery bins are then shifted to match that of the FC bins. However, the success of the synchronisations varied depending on the nature of the datasets. Some synchronisation results were less accurate than others, as demonstrated in Appendix A3. Nonetheless, the outcome of the BM and the verification is presented in Figure 3.6.

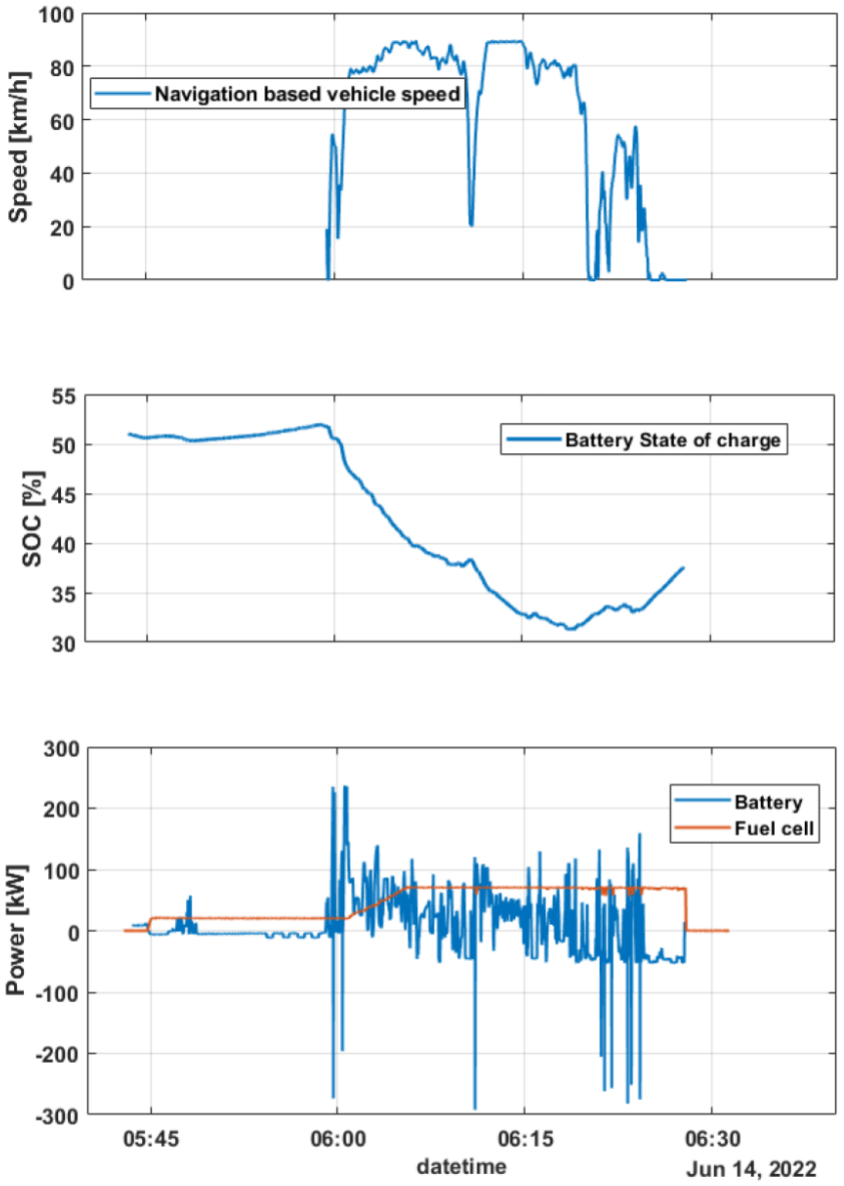

Figure 3.6. Synchronisation of result applying the BM on the Figure 3.4 data.

The synchronisation of the datasets can be verified by comparing the battery and FC power, battery SOC and vehicle speed. In this particular example, before 06:00 the FC is delivering power of about 20 kW, the battery power is in steady state below zero, the truck is standing still and the SOC is slowly increasing. Or in other terms, the FC charges the battery as the truck idles. After 06:00, the FC increases to about 80 kW, the battery operates dynamically, the truck is driving at high speeds (around 80 km/h) and the SOC is decreasing until the speed is low enough for the SOC to be charged by the FC and regenerative braking (as long as the speed has a negative derivative). The durations of the sets are aligned, hence, this synchronisation is confirmed. This was one synchronised set of files among many. The cases where the FC displayed dynamic behaviour the synchronisation became more difficult.

3.3 Test cycle development

The development of a typical FC test cycle was based upon previous research on ICE drive cycle development. In the referred studies the researchers employed the data clustering method on samples of real drive data by exercising the k-means clustering on micro-trips. [37]-[40] A micro-trip is commonly defined as the time series between two successive stops in the drive data. [40]

However, in this thesis a micro-trip will be similarly defined although as the sequence of FC operation between 0.01 kW of load requirement. Micro-trip data extraction enables the calculation of average power output and temperature for each micro-trip.

This section lays out the approach taken in developing the test cycle, highlighting the categorisation of modes of operation, adaptation of statistical techniques to capture the unique characteristics of a refuse FC truck and requirement on the validation of the test cycle. Beginning with the categorisation of the micro-trips.

3.3.1 Micro-trip categorisation

From the sample of synchronised data, the files with geo-coordinated data, vehicle speed and SOC data were considered useful for the categorisation. By mapping the geo-coordinates, as seen in Figure 3.7, the mode of driving and FC operation could be categorised. The FC refuse truck operation was categorised into “urban drive”, “non-urban” and “standing still” categories. “Urban driving” means that the truck was driving in Gothenburg city or in residential areas around Gothenburg city. “Non-urban driving” was when the truck was driving in industrial or rural areas outside of Gothenburg city. “Standing still” is when the truck is idling and the battery is being charged by the FC.

In some micro-trips the truck drove in both urban and non-urban. These micro-trips were assigned to the category of longer time duration. The categorisation of the micro-trips was done on the FC power profile. If the truck were standing still but the SOC changed as a result from a FC power output (i.e. battery is being charged by the FC) the power profile is labelled “Standing still”.

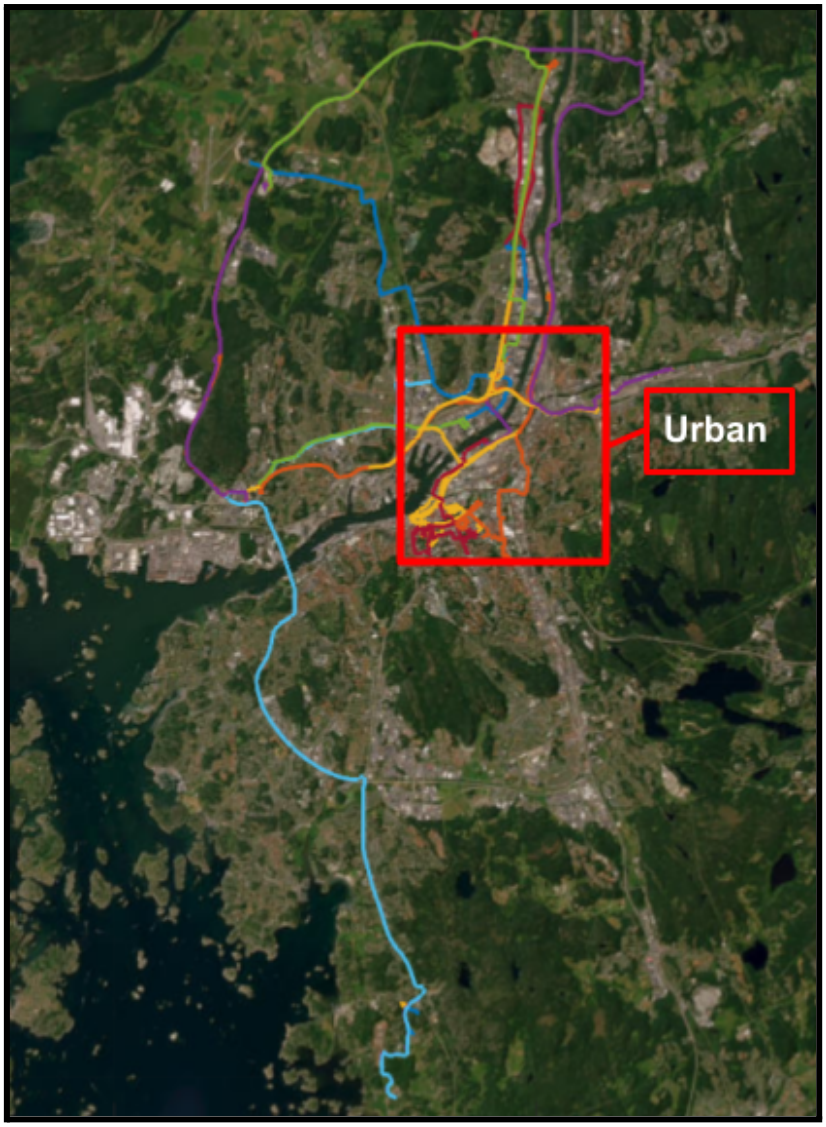

Figure 3.7 Geo-coordinates from the truck driving from a satellite view of Gothenburg. Plotted from MATLAB.

3.3.2 K-means clustering & Test cycle construction

To be able to create a typical test cycle representing the FC power output in a day of service from the pool of micro-trips, k-means clustering was explored. An existing function on MATLAB called “kmeans“ was used for the analysis. [41] K-means clustering is an unsupervised machine learning algorithm widely used for grouping or clustering data points. [40] The algorithm is briefly explained and is supported by a simple depiction of it, in Figure 3.8.

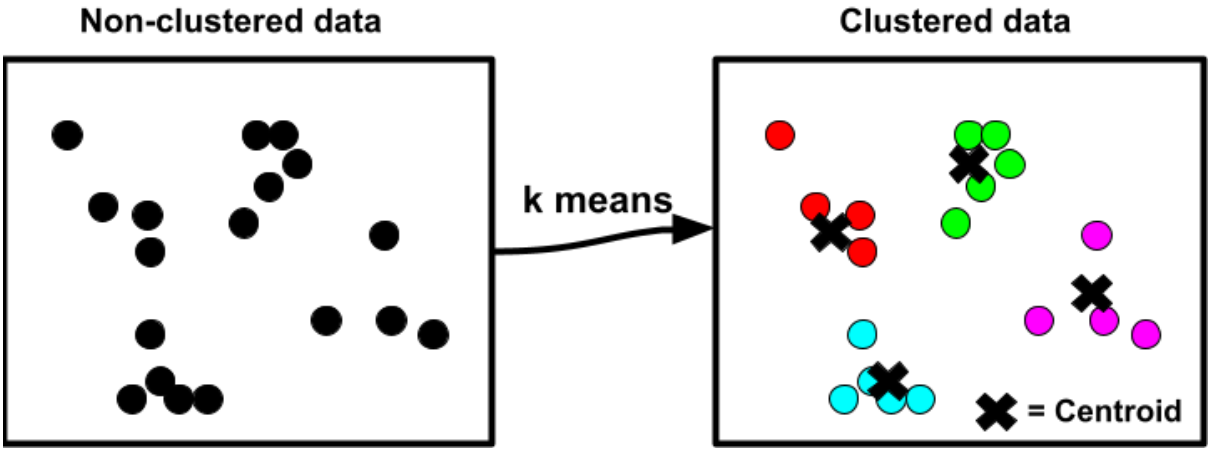

Figure 3.8 A simplified illustration of an input and output example of the k means clustering.

Initially, a desired number of k clusters is chosen. The algorithm proceeds to identify k centroids in the data space, each representing the centre of a cluster. Subsequently, every data point is assigned to the nearest centroid, forming k clusters. By calculating the mean of the data points within each cluster, the algorithm updates the centroids iteratively. Simultaneously, it re-assigns data points to the centroid closest to them. This iterative process continues until the centroids stabilise, meaning that the sum of squared errors of each centroid has been minimised. At this point, the algorithm has successfully grouped the data points into distinct clusters, see Figure 3.8. In summary, k-means clustering facilitates the automatic partitioning of data into clusters by iteratively adjusting centroids until an optimal clustering configuration is achieved. [42]

The k-means clustering was performed on extracted statistical features of each micro-trip. These features were the mean power and temperature. How the level dependence of the micro-trip categories can be seen in Appendix A4.

3.3.3 Validation strategy

The test cycle was constructed by assembling micro-trips from real drive data based on how representative the micro-trips were. The usage of the truck thus the FC power profiles could show different characteristics depending on the file's position in time. To make the test cycle representative of a day of operation the time duration of the FC power demand was considered an important aspect for validation of the test cycle. By meshing the files which belong to the same day of recording, the FC active time in one day was calculated. Between micro-trips, however, a 16-minute pause was added. This was based on a manual inspection of files which detected that they were common files of test driving.

3.4 Fuel cell performance

Since this is a pilot study and up until April 2023 the refuse truck has not been in official service, the FC duty has been different from the start of the FC refuse truck project. It was therefore important to have an overview of the FC power demand through time. Which power level was requested more often depending on the position in time. Additionally, the total time of active FC power request was calculated.

Polarisation curves of all the micro-trips, including the coolant average temperature of each data point, were prepared. Beginning of life (BOL) polarisation curves of the FC were provided from PowerCell. The BOL-data points were included for reference.

The quantification of FC ageing was based on the micro-trips. Due to the limitations of the data and the available variables, FC ageing was approximated as the deterioration of isothermal FC power corresponding to a low, medium and high current. The levels of current investigated were 50, 125, 200 and 250 A.

3.5 Additional data

In the end stage of this thesis project, data recorded from the end of March 2023 to the beginning of May 2023 was provided to this research. From the beginning of April 2023 to May 2023, the truck collected cardboard material. Instead of applying the same data-filtering all of the new FC- and battery power were plotted. Contrary to the previous data recordings, the difference between the FC and the battery data was almost a fixed value: about 33 minutes. The BOL data was supplied to this work pool of data at the end stage of the project; due to the quality of the data it was not processed to be included in the micro-trip database.

4. Results

This section presents the results obtained from analysing the two datasets covered, although they might not be representative of a typical refuse truck in service. Throughout the pilot study, test driving, maintenance, and some refuse material collection were conducted. However, due to data discrepancies, not all of these activities were captured accurately. It is also worth mentioning that the main focus of this thesis lies in the methodologic approach which can be easily reproduced for new sets of data that will be collected in the future. The following section will address the research questions and the additional data.

4.1 Research question 1: Test cycle

The figures and data presented in this section are the results answering research question 1:

1. *Development of a test cycle that ought to represent a typical single day driving pattern followed by the truck.*

Micro-trip categorisation resulted in 19 Standing still, 27 Non-urban and 41 Urban micro-trips. Examples of labelled micro-trips can be seen in Figures 4.1 and 4.2. These include all of the micro-trip categories. However, the standing still category is not labelled, since it constitutes a minor part of the micro-trip in Figure 4.1. More micro-trip examples can be found in Appendix A4.

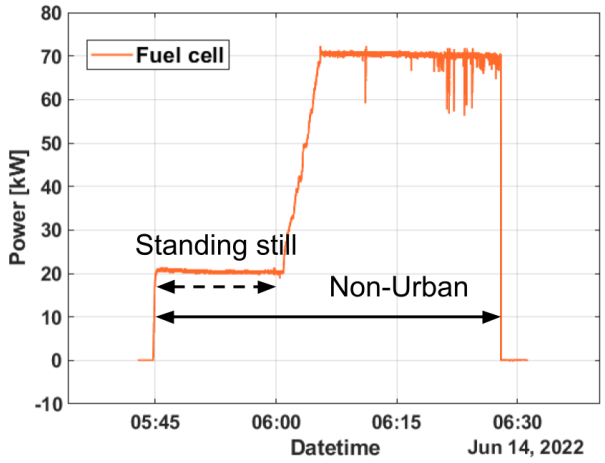

Figure 4.1 Micro-trip consisting urban and standing still (05:45-06:00). Non-Urban accounts for the majority of the time.

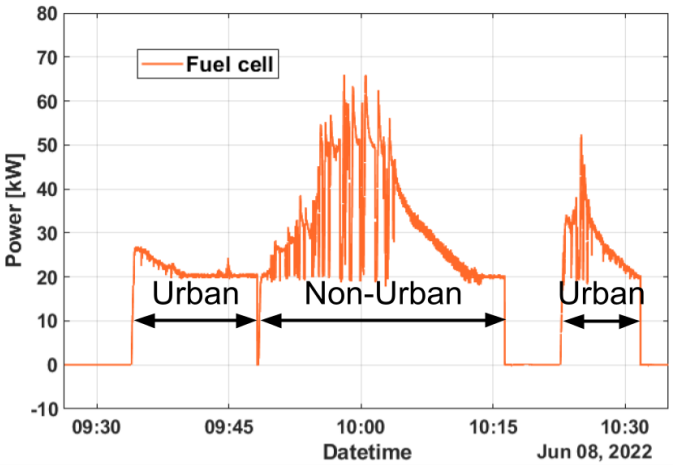

Figure 4.2 Two urban and one Non-urban micro-trips.

Figures 4.1 and 4.2 (and the examples in Appendix A4) reveal the diversity of the FC power profiles. Standing still are seen to account for steady state FC power requests whereas urban

micro-trips can be both steady state and dynamic. Non-urban samples, on the other hand, display a similar dynamic power profile as urban micro-trips, although at higher power. Moreover, these categories were used as a database for the k-means clustering. The k-means clustering was performed on extracted statistical features of each micro-trip (i.e. the mean power and temperature). This resulted in the graph seen in Figure 4.3.

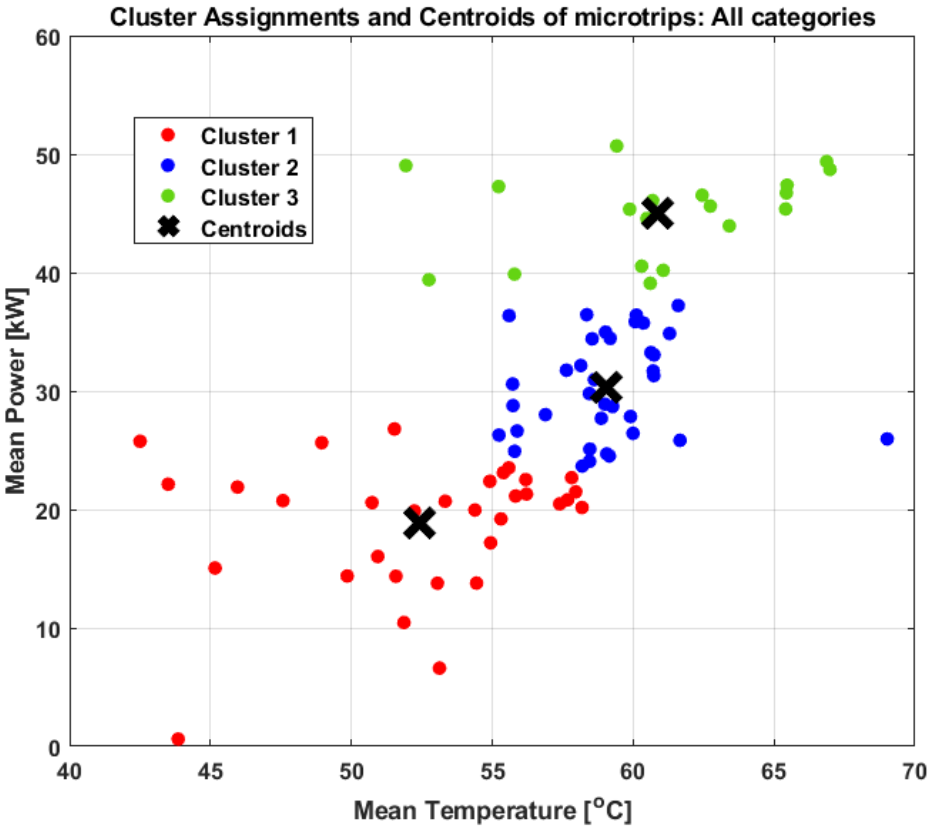

Figure 4.3 K-means clustered micro-trips mean power vs mean temperature.

A value of k = 3 was chosen thus the k-means algorithm computes three clusters. The number was chosen as an initial guess based on the three categories of the micro-trips. The three clusters represent low, medium and high power and temperature mode of operation. Performing an evaluation of the clusters in Figure 4.3 revealed that the optimal number of clusters were equal to 4. This is due to the outliers closest to the graph axis. By manually removing the two outliers, the cluster evaluation resulted in an optimal number of clusters of 3. Hence, the analysis continued with the extraction of the three modes FC operation.

The centroids in Figure 4.3 correspond to the arithmetic mean of the points of each cluster [42]. The points closer to the centroids are considered more representative to that cluster implying that they are more representative to that mode of operation. The micro-trips corresponding to the points closest to the centroids are used for assembling the test cycle. To

eliminate background noise in the data for the test cycles the data was smoothed. This was done with the moving median smoothing,"smoothdata" function on MATLAB, at a step size of 10. [43]

As was stated in the Methodology chapter, when constructing the test cycle the more representative micro-trips of the micro-trip category i.e. micro-trips close to the centroids of each cluster ought to be chosen. What is presented in Figure 4.4 consists of the micro-trips closest to their centroids.

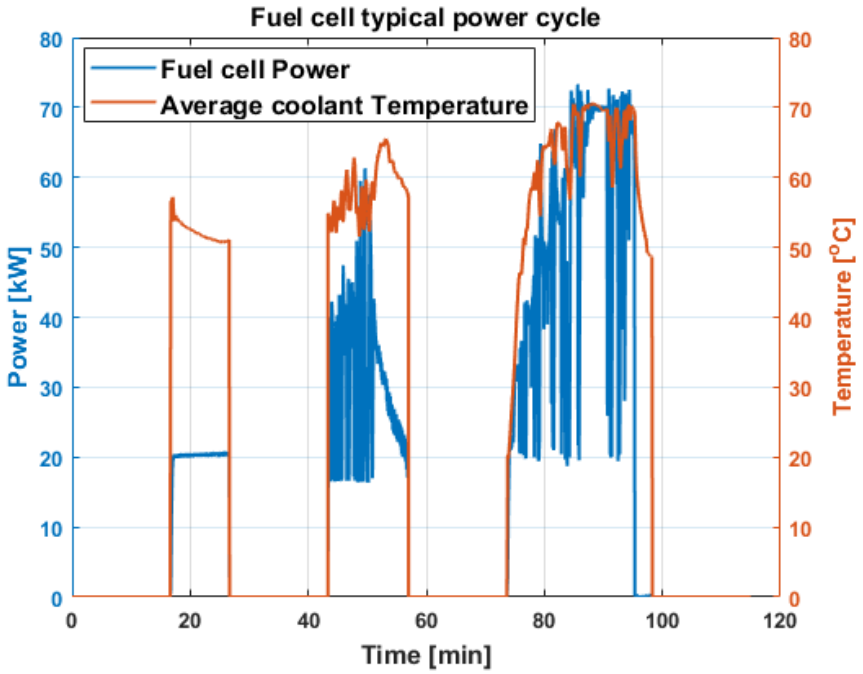

Figure 4.4 A test cycle constructed from the k-means clustering. In this conformation it consists of the FC power and temperature.

Three micro-trips were meshed together with a pause of about 16 minutes between the FC operation. Starting from the left to the right in Figure 4.4; the first duty is a steady state power output from the standing still category or the low power mode of operation. Its duty represents charging the battery only with a power request of 20 kW at around 50℃. This is how most power cycles in the standing still cluster appear. The subsequent FC duty is of the urban drive category or medium power mode. It displays a dynamic power profile. FC power to assist the battery with charging, auxiliary components and the EMU is requested. This dynamic power profile is typical of its cluster as it ranges around 20-60 kW at 55-65℃. However, some can consist of steady state segments (representing either standing still or driving of the truck). Lastly, non-urban (highway) driving or high-power mode of operation. The difference to urban driving is that more power (70 kW) is requested from the FC to the EMU thus higher temperatures are reached as well, 70℃. Similarly to urban driving, some non-urban

micro-trips too consist of steady state power requests. Both Figure 4.1, 4.2 and Appendix A4 show examples of these. However, it is important to note that the duration of the micro-trips are different from each other. Moreover, the duration of FC power request in this test cycle is about 50 minutes. Total time of the test cycle, including pauses, is approximately 80 minutes.

By meshing the files which belong to the same day of recording, the FC active time in one day was calculated. FC active in this case P > 0.01 kW. The mean FC active time spent in the files in the light blue and yellow domain in Figure 3.1 was calculated to be 1.07 hours. Hence, ~1 hour of FC operation is more probable, ergo the test cycle FC active time should match that duration. However, between micro-trips a 16 minute pause was added. This was based on a manual inspection of files which detected that they were common files of test driving.

4.2 Research question 2: Fuel cell ageing

The figures and data presented in this section are the results answering research question 2:

2. *Quantification and, if possible, forecasting of degradation/ageing of the fuel cell performance in this pilot truck.*

The bar graph presented in Figure 4.5 aims at showing how different intervals of FC power requests have occurred in time. Or in other terms, a stacked bar plot showing the relative frequency of FC power levels throughout 2020 to 2023. The darker colours belong to the older data and the brighter closer to the first quarter of 2023. More than half of the time the FC was inactive i.e. zero power request (second bar to the left). Looking at its colour gradient, a wide interval of green corresponding from late 2021 to end of 2022 constitutes of inactive FC operation time. Moreover, power requests around 90-100 kW only occurred in 2020, which, as was revealed in the interview, corresponded to FC testing data recordings. In the newest data from 2023 the power requests of higher frequency are shown to be in the 00-30 kW range, however all the power ranges between 0 and 80 kW are recorded, confirming that various driving modes correspond to different power outputs.

The amount of time when the FC requested power, in this case defined as P > 0.01 kW. The total time of FC data recording is 3814.2 hours and in that time the FC has been active for 141.80 hours between 2020-2023.

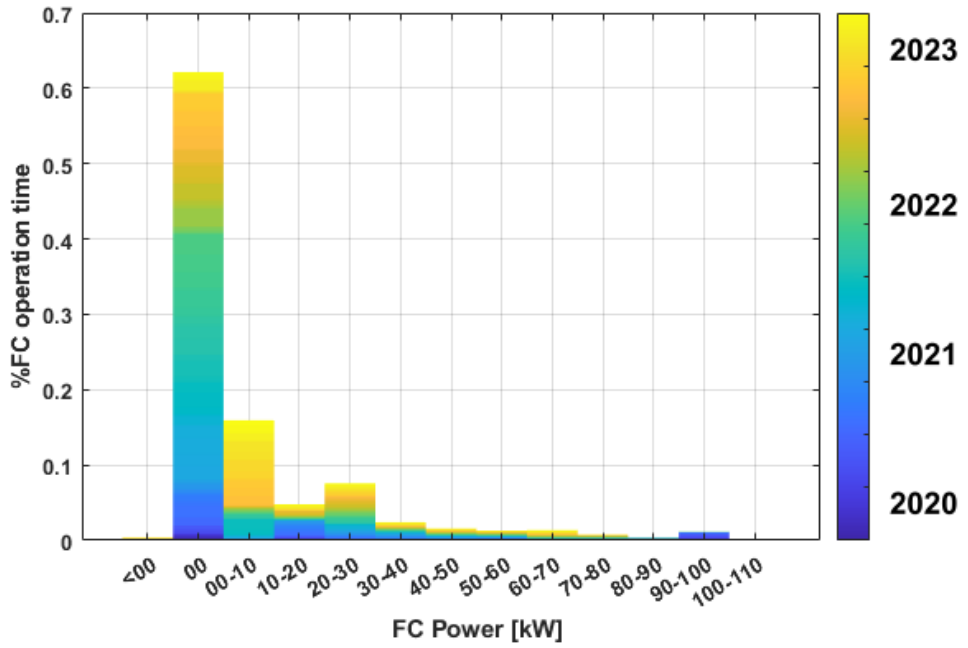

Figure 4.5 Distribution of Power intervals through time.

A polarisation curve was made, referring to Figure 4.6. It contains the average cell voltage of all the micro-trips together with the BOL data points from Table 4.1 for reference. BOL values are shown in Table 4.1. The cell voltage, E_{Cell} [V], was calculated by dividing E_{BOL} [V], from the table, with the number of cells in the FC stack.

Table 4.1 Beginning of life data points of the FC.

$E_{BOL,\ stack}$ [V]	369	346	337	328	319	314
$I_{BOL,\ stack}$ [A]	45	100	150	200	250	300
$E_{BOL,\ cell}$ [V]	0.810	0.760	0.741	0.721	0.701	0.690
$P_{BOL,\ gross}$ [kW]	17	35	50	65	79	93
$P_{BOL,\ net}$ [kW]	15	33	48	60	72	84

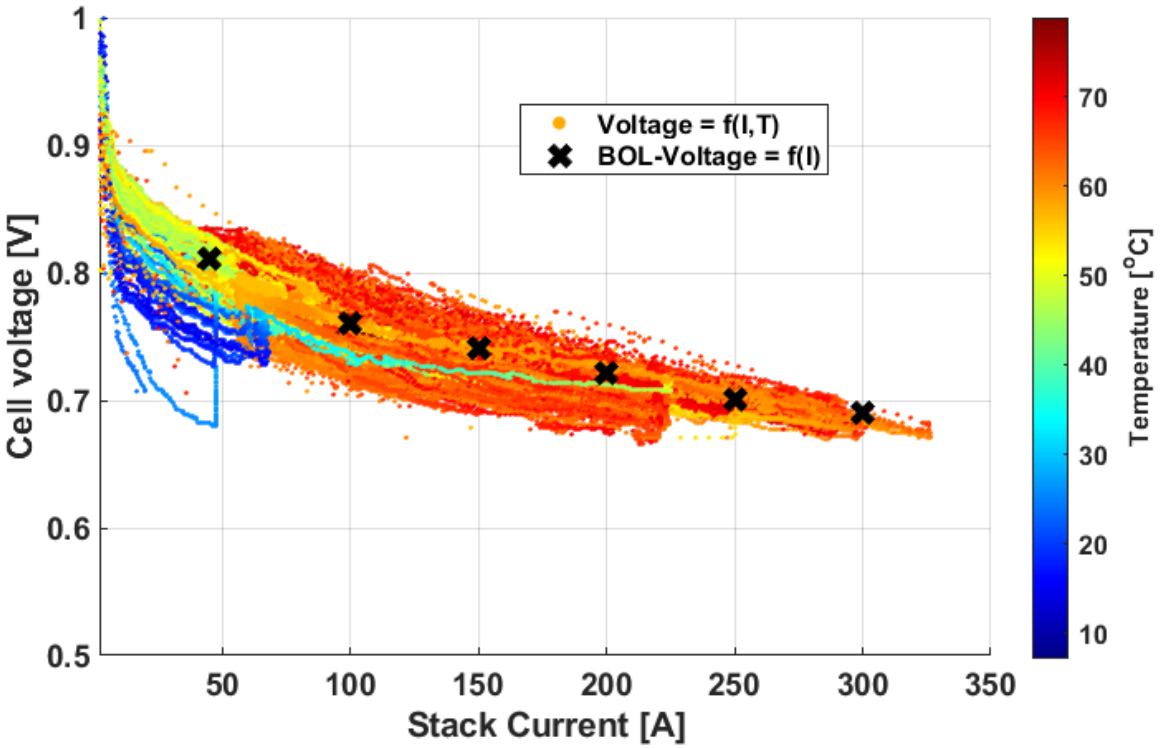

Figure 4.6 Polarisation curves from every micro-trip. Constructed by average cell voltage and stack current. Temperature bar graph is included to display the temperature distribution.

It is important to note that the pool of micro-trips consisted of 19 Standing still, 27 Non-urban and 41 Urban micro-trips. At higher currents, the polarisation curves are within a quite narrow voltage range and they exhibit almost a uniform temperature distribution; reaching temperatures of 60 ℃. In the mid-section (i.e. 70-230 A) the uniformity begins to break up as both the temperature and current transitions to lower magnitudes. A turquoise curve is shown in that region belonging to even lower temperatures (30-40 ℃) than points at the same currents. In the current interval of 0-70 A, a broad diversity of temperatures can be seen, appearing in the range of 10-60 ℃, probably recorded during start-ups. Overall the temperature increases with higher currents, this can be seen in the smooth transition from cold to warmer colours e.g. turquoise curve in the mid region. The equation (VIII) was defined as: $P = E_{Stack} \cdot I_{Stack}$. Lower current region corresponds to lower power and vice versa. Within the low current region at 50 A, voltages at 70 ℃ stand out among the others which are around 50 ℃.

A plot was made on the same files that passed the criteria when constructing Figure 4.5. It contains the current level distributions through time, similar to Figure 4.5. This bar graph can be seen in Figure 4.7. It shows that the FC was requested for high loads (280-320 A), similar

to Figure 4.5. Closer towards 2023 low to medium current demands become more prominent (currents ranging between 40 to 240 A).

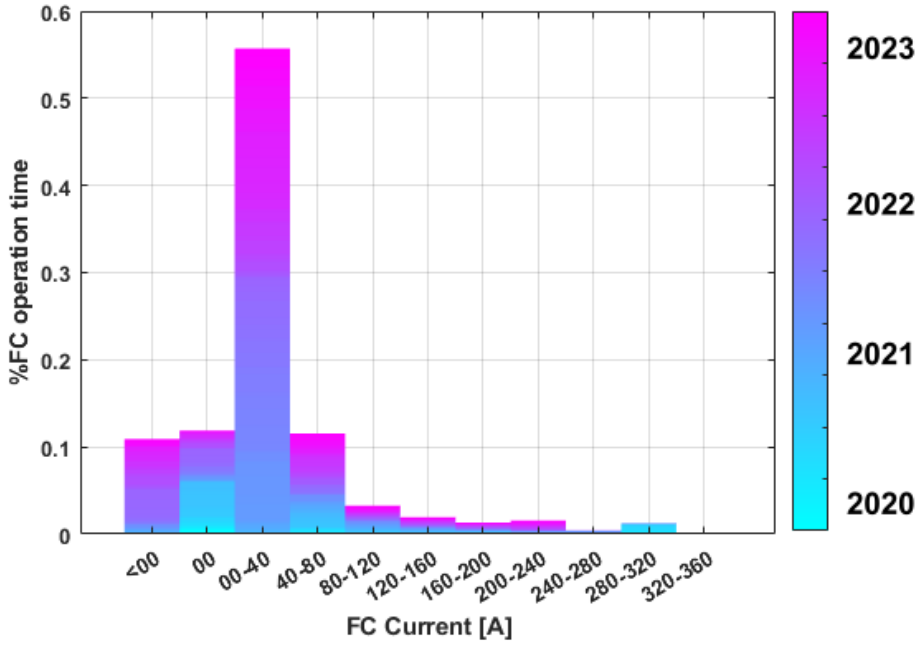

Figure 4.7 Distribution of Current intervals through time.

The last result in this section pursues quantifying degradation of FC performance. In this case it is the decline of FC power at constant currents and the temperature range [40,80]℃. The scatter plot shown in Figure 4.8-4.11 presents micro-trips mean iso-current FC power. The constant currents are 50, 125, 200 and 250 A. Each point in the figures represents a micro-trip in time. A bar graph that sets out the colour code of the data points is included (i.e. points of a certain colour represent a temperature).

What can be seen in all of the Figures 4.7-4.10, is that for the same currents and temperatures the power may vary. For example, in Figure 4.7 the deep blue power in April 2021 (~17.8 kW) is lower than the point at the same temperature in July 2022 (~18.3 kW). In Figure 4.8-4.11 do the lime green points corresponding to about 59 ℃ hardly show any decrease in power at the same currents between 2021 and 2022. In contrast, the FC at these currents and temperatures demonstrates somewhat higher values in 2022.

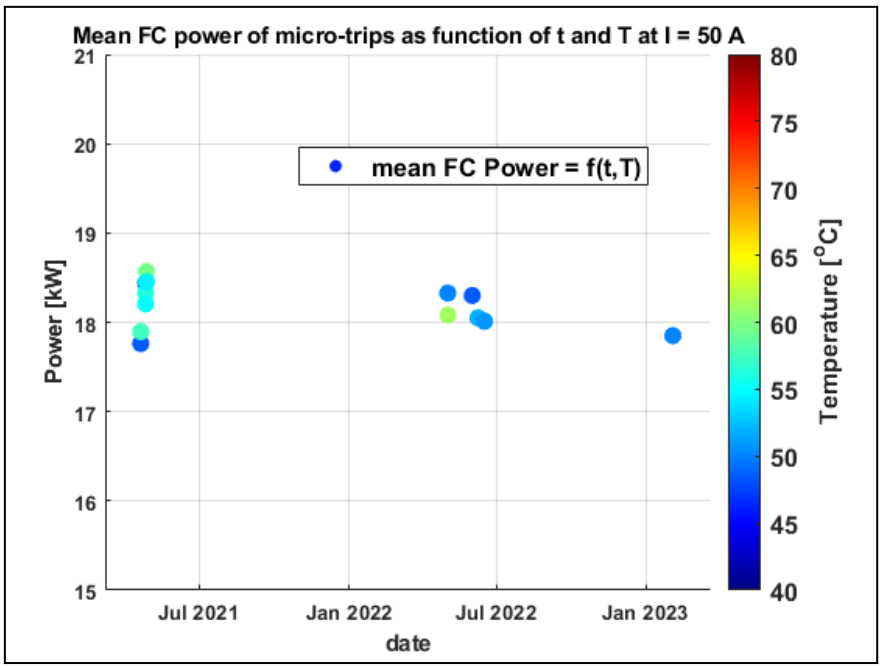

Figure 4.8 Scatter plot of the mean power of micro-trips with data at I = 50 A and T = [40,80]℃

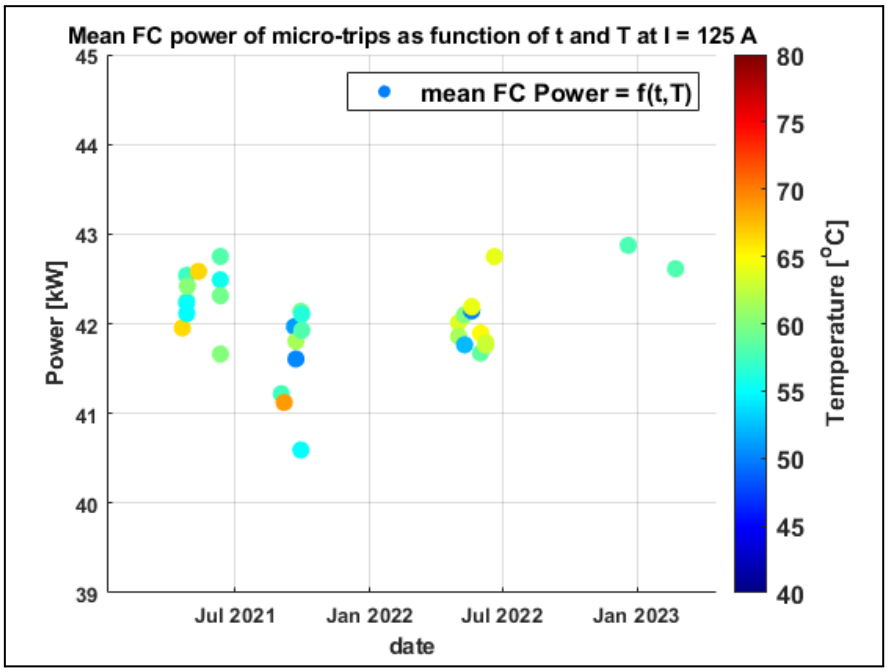

Figure 4.9 Scatter plot of the mean power of micro-trips with data at I = 125 A and T = [40,80]℃

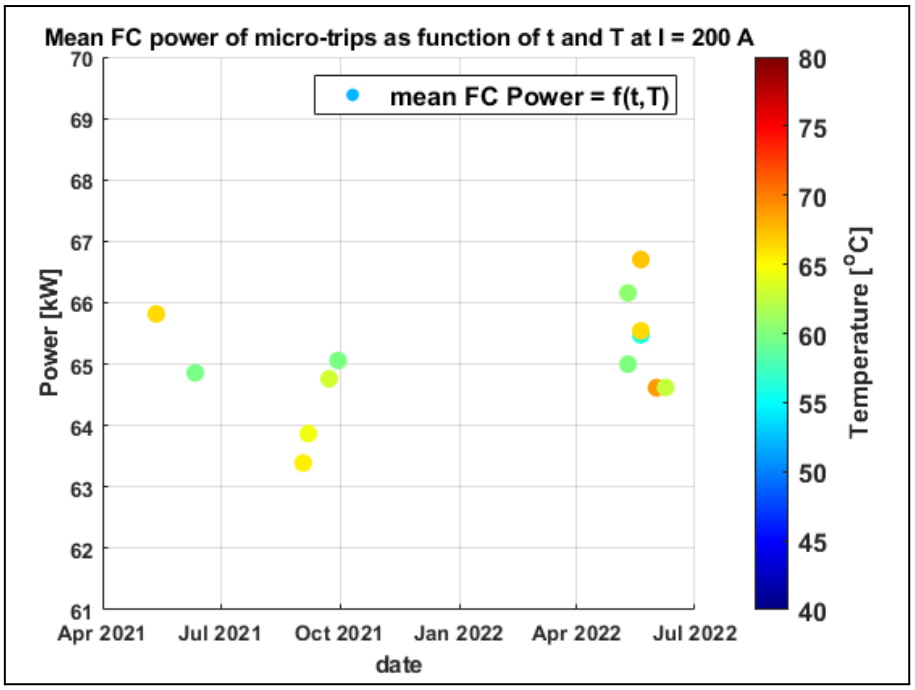

Figure 4.10 Scatter plot of the mean power of micro-trips with data at I = 200 A and T = [40,80]℃

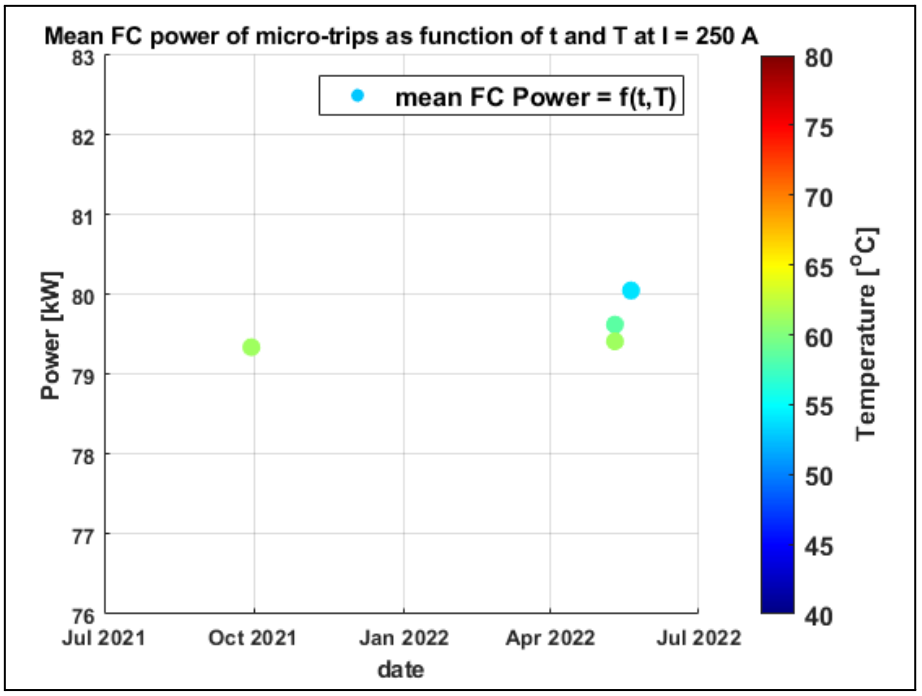

Figure 4.11 Scatter plot of the mean power of micro-trips with data at I = 250 A and T = [40,80]℃

The figures and data presented in sections 4.1 and 4.2 the results attempting to answer research questions 1 and 2. These are discussed in the subsequent Discussion chapter. However, prior to that an overview of the additional real drive data collected between mid of March 2023 and beginning of May 2023 will be presented in the following section.

4.3 Additional data

The data recorded from the middle of March 2023 to the beginning of May 2023 was looked upon. The plot shown in Figure 4.12 consists of the power outputs from both battery and FC. The S-set files, battery data, are monochromatic, red, in the figure. However, the S-set files are distinct from each other in time as can be seen in the figure. The FC-set files, on the other hand, are assigned individual colours exclusive from the adjacent FC-files. What can be seen in Figure 4.12 is that FC-set data is missing when the S-set exhibits data recording. The prominent example of this is the FC gap seen in April. Gaps such as that are a new phenomenon in the data. The FC data recordings which are empty (i.e. P(max) = 0 kW) can still be seen between March and April. Because of the impossibility of synchronising the data in time, these data were not taken into consideration for the work.

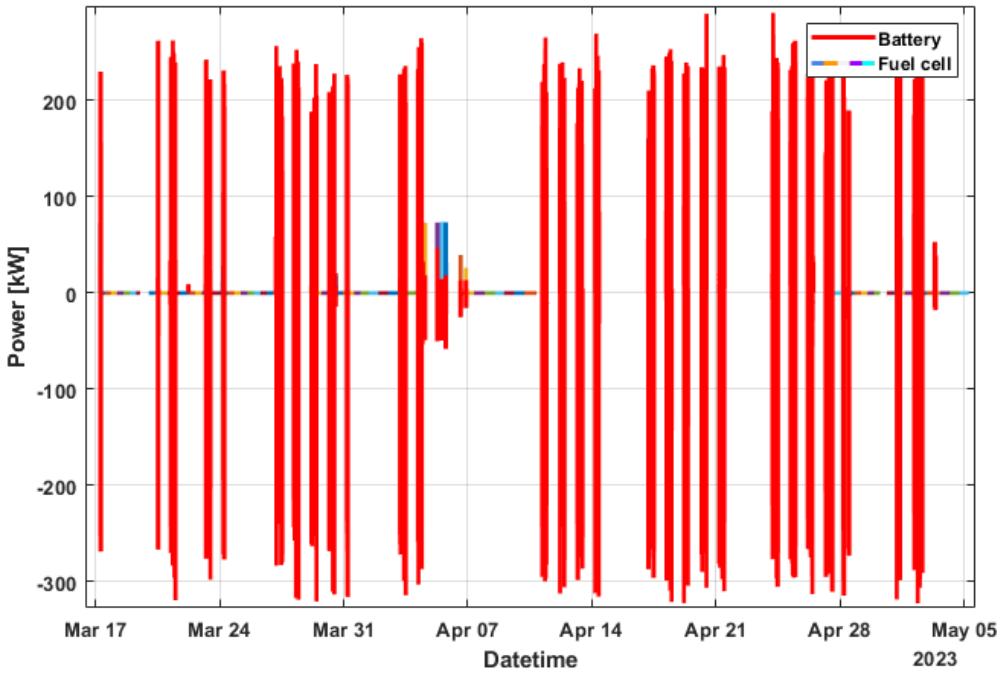

Figure 4.12 Daily FC- and battery power from March 17th to May 5th.

5. Discussion

The chapter follows the same structure as the results chapter. Beginning with commenting on the results attempting to answer research question 1 and later research question 2. Then it closes up with a final comment on the additional data.

5.1 Research question 1

It has been emphasised throughout the report that this study was on a pilot truck. The usage profile of the refuse truck, referred to as Albert, is time-dependent, as evidenced by the FC power profiles presented in Appendix A1 and A4. The data contains files pertaining to FC testing or test driving, but no indications of mass collection or compression activities have been identified, as previously mentioned. Consequently, the test cycle does not fully capture the operational conditions of a refuse truck in service. However, it does provide a mean power profile of the FC refuse truck during the period spanning from early 2020 to March 2023. Furthermore, as conveyed by the truck driver during the interview, since this vehicle type is relatively new, future drivers have to familiarise themselves with its operation. This factor may contribute to the variance observed in the power profiles. Nonetheless, it is important to acknowledge that this project remains ongoing, and additional data will be collected as the refuse truck transitions into actual service duties. These data can be analysed with the established methodology.

The test cycle presented in the results section represents one of the possible test cycles obtained through the utilisation of k-means clustering on "micro-trips" or FC power cycles. Figure 4.4 illustrates a power and temperature profile, but it is possible to include voltages, currents, and reactant gas pressure depending on the specific stressors targeted by the test cycle. This test cycle is derived from real drive data, encompassing both steady-state and dynamic FC behaviour. Consequently, it incorporates stressors such as SU/SD sequences, potential cycling, and temperature fluctuations (as shown in Figure 2.3), which may contribute to MEA failure. However, the assumption regarding the FC temperature and the overall suitability of the test cycle still require verification.

Further refinement of the test cycle is required. For instance, when comparing it with load cycles depicted in Figures 2.4-2.6, the presented test cycle exhibits a shorter duration compared to the DOE and NEDC protocols, but is similar to the ID-FAST protocol. All of these protocols entail more power cycles and SU/SD sequences. However, it is important to

note that the real drive-based test cycle offers greater dynamic representation. Additionally, the frequency of testing plays a crucial role in constructing ASTs or test cycles, an aspect that warrants further investigation in future work. [44] In summary, this work serves as a foundational step towards the comprehensive evaluation of the FC refuse truck.

5.2 Research question 2

Most of the time throughout 2020 to 2023 the FC has been inactive, seen in Figure 4.5. However, there are occasions in which the FC shows dynamic behaviour as seen in the FC power profiles. This is most likely due to sudden power requests from auxiliary devices in the vehicle. The fraction of the FC power that is delivered to auxiliary components used for collecting the garbage is not logged in the data, so it could not be used in this work to differentiate the work spent to move the tuck from the work spent to collect the garbage. The FC power demand has changed with time, revealed by Figure 4.5. The 90-100 kW power outputs occurring around 2020 implies testing was conducted around then. Such examples can be seen in Appendix A2.

In Figure 4.6 the cell voltage is shown as a function of current and temperature. It displays the behaviour that can be seen in the theoretical polarisation curve in Figure 2.1. Figure 4.6 shows that the FC is employed mainly in the high-middle voltage region (supported by the low to medium current levels in Figure 4.7). In fact, the polarisation curve does not reach the concentration polarisation region at high currents (i.e. where voltage slope increases sharply as seen in Figure 2.1). This shows that the FC is operated within the higher efficiency region. Less entropic heat ($T\Delta S$) is generated for the same work generated at higher currents. The cell voltages Figure 4.6 transitions from lower to higher temperatures at higher currents. This validates the temperature assumption that was made i.e. FC temperature constitutes to the average coolant temperature in Table 3.1. The coolant, after all, absorbs the entropic heat from FC activity. Looking again at the temperature distribution in Figure 4.6, the same temperatures (about 60-70℃) can appear at currents of 70-320 A. Considering the fact that the Hydrogen consumption is larger at higher currents, more thermal energy is therefore released. The same FC temperature at lower to higher Hydrogen gas consumption rates indicates that the thermal management system is effectively the heat generated by the FC.

Colder temperatures, e.g. 00-30℃, can be seen in the polarisation curves. This is most likely artefacts from the truck standing outside in winter season and the FC is starting up. The polarisation curves also reach around 350 A which corresponds to around 90 kW. The FC

testing power profiles in Appendix A2 from 2020 show such behaviour. The region in Figure 4.5 at 200 A contains more modern data. This is supported by Figure 4.7 when looking at the colour code of the 200-240 A bar.

No sign of degradation could be detected in the Figures 4.7-4.10. This is due to the fact that the temperature and current did not show any kind of trend of that sort on the power. External factors such as the operator and the climate might influence the dispersion of the FC powers at the same temperature and currents. On the other hand, the FC has only been active for 141.80 hours in the data evaluated. Lifetimes of FCs in HD vehicles today, as has been stated, are fixed at 25,000 hours and above. At this stage, more time and truck operation is still needed until FC deterioration can be observed.

5.3 Additional data

The FC data collected between March 2023 and May 2023 cannot be of use due to the absence of overlapping dataset from the 2 loggers, probably due to lost segments in both the datasets. If these types of trends reoccur, valuable data might not be recovered. April 2023 was the time when the FC actually began to collect refuse material and therefore that period corresponds to the most useful data in terms of usage patterns for the collection of the cardboard material. Although the data are sparse and not usable, the fact that the truck is functional for the garbage collection is a milestone in the project.

6. Remarks and conclusions

In conclusion, this pilot investigation has provided a mean power profile of the FC refuse truck, Albert, from early 2020 to March 2023, offering valuable insights into its usage profile. Although the test cycle does not fully capture real service conditions, it serves as a foundational step towards evaluating the FC refuse truck. The observed variance in power profiles can be attributed to the learning process of new drivers, highlighting the need for ongoing data collection as the truck transitions to actual service duties. Further refinement of the test cycle and investigation into testing frequency are recommended for future research.

Regarding the analysis of FC power profiles, the truck exhibited both steady-state and dynamic behaviour over the 2020-2023 period, likely due to sudden power requests from auxiliary devices. However, distinguishing between work spent on vehicle movement and garbage collection was challenging due to the lack of data on power allocation. The FC power demand showed temporal changes, including higher outputs around 2020 during testing. The behaviour of cell voltage aligned with the theoretical polarisation curve, confirming the FC's operation within a high-efficiency region. While timely aspects were captured in the polarisation curves, no degradation was observed in the evaluated data. Extended truck operation and monitoring are needed to observe FC deterioration as the current data represents only a fraction of the FC's expected lifetime.

Overall, the refuse FC truck can be concluded to be a successful project. The truck driver expressed his positive impressions of the refuse truck when being interviewed, after collecting refuse material in April 2023. An additional Hydrogen refuelling station will be put in place in 2023, expanding the Hydrogen gas infrastructure Gothenburg. Taking these into account highlights the potentials refuse FC trucks possess.

Bibliography

[1] Regeringen och Regeringskansliet, “Sweden’s climate policy framework,” *Regeringskansliet*, Mar. 11, 2021. https://www.government.se/articles/2021/03/swedens-climate-policy-framework/ (accessed June. 01, 2023).

[2] “Sveriges utsläpp och upptag av växthusgaser.” https://www.naturvardsverket.se/data-och-statistik/klimat/sveriges-utslapp-och-upptag-av-vaxthusgaser/ (accessed June. 01, 2023).

[3] “Reducing CO_2 emissions from heavy-duty vehicles,” *Climate Action*. https://climate.ec.europa.eu/eu-action/transport-emissions/road-transport-reducing-co2-emissions-vehicles/reducing-co2-emissions-heavy-duty-vehicles_en (accessed Jun. 01, 2023)

[4] ‘Hydrogen fuel cell heavy-duty trucks: Review of main research topics - ScienceDirect’. https://www.sciencedirect.com/science/article/abs/pii/S0360319922029068 (accessed Feb. 07, 2023).

[5] E. Masovic, “Vätgasbilen – världens renaste sopbil,” *JOAB*, Jun. 2021, [Online]. Available: https://www.joab.se/vatgasbilen-varldens-renaste-sopbil/ (accessed Jun. 01, 2023)

[6] Y. Wang, D. F. Ruiz Diaz, K. S. Chen, Z. Wang, and X. C. Adroher, ‘Materials, technological status, and fundamentals of PEM fuel cells – A review’, Mater. Today, vol. 32, pp. 178–203, Jan. 2020, doi: 10.1016/j.mattod.2019.06.005.

[7] ‘A review of durability test protocols of the proton exchange membrane fuel cells for vehicle’, Appl. Energy, vol. 224, pp. 289–299, Aug. 2018, doi: 10.1016/j.apenergy.2018.04.050.

[8] S. Pardhi, S. Chakraborty, D.-D. Tran, M. El Baghdadi, S. Wilkins, and O. Hegazy, ‘A Review of Fuel Cell Powertrains for Long-Haul Heavy-Duty Vehicles: Technology, Hydrogen , Energy and Thermal Management Solutions’, Energies, vol. 15, no. 24, Art. no. 24, Jan. 2022, doi: 10.3390/en15249557.

[9] P. Pei and H. Chen, ‘Main factors affecting the lifetime of Proton Exchange Membrane fuel cells in vehicle applications: A review’, Appl. Energy, vol. 125, pp. 60–75, Jul. 2014, doi: 10.1016/j.apenergy.2014.03.048.

[10] ‘Regler om kör- och vilotider - Transportstyrelsen’. https://www.transportstyrelsen.se/sv/vagtrafik/Yrkestrafik/Kor--och-vilotider/regler-om-kor--och-vilotider/ (accessed Feb. 07, 2023).

[11] J. Kunze-Liebhäuser, O. Paschos, S. S. Pethaiah, and U. Stimming, ‘Fuel Cell Comparison to Alternate Technologies’, in Fuel Cells and Hydrogen Production, T. E. Lipman and A. Z. Weber, Eds. New York, NY: Springer New York, 2019, pp. 11–25. doi: 10.1007/978-1-4939-7789-5_157.

[12] ‘Accelerated Membrane Durability Testing of Heavy Duty Fuel Cells - IOPscience’. https://iopscience.iop.org/article/10.1149/2.0671501jes (accessed Feb. 07, 2023).

[13] C.-Y. Hsieh, P. Pei, Q. Bai, A. Su, F.-B. Weng, and C.-Y. Lee, ‘Results of a 200 hours lifetime test of a 7 kW Hybrid–Power fuel cell system on electric forklifts’, Energy, vol. 214, p. 118941, Jan. 2021, doi: 10.1016/j.energy.2020.118941.

[14] About Revive’, *Revive*. https://h2revive.eu/about-revive/ (accessed Feb. 07, 2023).

[15] F. Barbir, ‘CHAPTER 2 - Fuel Cell Basic Chemistry and Thermodynamics’, in *PEM Fuel Cells*, F. Barbir, Ed. Burlington: Academic Press, 2005, pp. 17–32. doi: 10.1016/B978-012078142-3/50003-3.

[16] F. Barbir, ‘CHAPTER 3 - Fuel Cell Electrochemistry’, in *PEM Fuel Cells*, F. Barbir, Ed. Burlington: Academic Press, 2005, pp. 33–72. doi: 10.1016/B978-012078142-3/50004-5.

[17] D. Hissel and M. C. Pera, ‘Diagnostic & health management of fuel cell systems: Issues and solutions’, *Annu. Rev. Control*, vol. 42, pp. 201–211, Jan. 2016, doi: 10.1016/j.arcontrol.2016.09.005.
[18] S. S. Araya, N. Li, and V. Liso, ‘Chapter 9 - Degradation and failure modes in proton exchange membrane fuel cells’, in *PEM Fuel Cells*, G. Kaur, Ed. Elsevier, 2022, pp. 199–222. doi: 10.1016/B978-0-12-823708-3.00015-8.
[19] ‘FCSys’. https://build.openmodelica.org/Documentation/FCSys.html (accessed Feb. 06, 2023).
[20] F. Barbir, ‘CHAPTER 1 - Introduction’, in *PEM Fuel Cells*, F. Barbir, Ed. Burlington: Academic Press, 2005, pp. 1–16. doi: 10.1016/B978-012078142-3/50002-1.
[21] “Comparison of Fuel Cell Technologies,” *Energy.gov*. https://www.energy.gov/eere/fuelcells/comparison-fuel-cell-technologies (accessed Feb. 06,2023).
[22] H. Tang, S. Peikang, S. P. Jiang, F. Wang, and M. Pan, ‘A degradation study of Nafion proton exchange membrane of PEM fuel cells’, J. Power Sources, vol. 170, no. 1, pp. 85–92, Jun. 2007, doi: 10.1016/j.jpowsour.2007.03.061.
[23] Ž. Penga, G. Radica, and F. Barbir, ‘Degradation Mechanisms in Automotive Fuel Cell Systems’.
[24] R. Banan, A. Bazylak, and J. Zu, ‘Combined effects of environmental vibrations and hygrothermal fatigue on mechanical damage in PEM fuel cells’, Int. J. Hydrog. Energy, vol. 40, no. 4, pp. 1911–1922, Jan. 2015, doi: 10.1016/j.ijhydene.2014.11.125.
[25] K. Yasuda, A. Taniguchi, T. Akita, T. Ioroi, and Z. Siroma, ‘Platinum dissolution and deposition in the polymer electrolyte membrane of a PEM fuel cell as studied by potential cycling’, Phys. Chem. Chem. Phys., vol. 8, no. 6, pp. 746–752, Feb. 2006, doi: 10.1039/B514342J.
[26] H. Pourrahmani et al., ‘A Review on the Long-Term Performance of Proton Exchange Membrane Fuel Cells: From Degradation Modeling to the Effects of Bipolar Plates, Sealings, and Contaminants’, Energies, vol. 15, no. 14, Art. no. 14, Jan. 2022, doi: 10.3390/en15145081.
[27] D. A. Cullen et al., “New roads and challenges for fuel cells in heavy-duty transportation,” Nature Energy, vol. 6, no. 5, pp. 462–474, Mar. 2021, doi: 10.1038/s41560-021-00775-z.
[28] J. Zhao and X. Li, ‘A review of polymer electrolyte membrane fuel cell durability for vehicular applications: Degradation modes and experimental techniques’, Energy Convers. Manag., vol. 199, p. 112022, Nov. 2019, doi: 10.1016/j.enconman.2019.112022.
[29] N. Garland, T. Benjamin, and J. Kopasz, ‘DOE Fuel Cell Program: Durability Technical Targets and Testing Protocols’, ECS Trans., vol. 11, no. 1, p. 923, Sep. 2007, doi: 10.1149/1.2781004.
[30] G. Tsotridis, A. Pilenga, G. D. Marco, and T. Malkow, ‘EU HARMONISED TEST PROTOCOLS FOR PEMFC MEA TESTING IN SINGLE CELL CONFIGURATION FOR AUTOMOTIVE APPLICATIONS’.
[31] ‘Investigations on degradation mechanisms and Definition of protocols for PEM Fuel cells Accelerated Stress Testing | ID-FAST Project | Fact Sheet | H2020 | CORDIS | European Commission’. https://cordis.europa.eu/project/id/779565 (accessed Feb. 07, 2023).
[32] ‘id-fast-image1-protocols-autostackprofiles.png (2004×1122)’. https://cordis.europa.eu/docs/results/h2020/779/779565_PS/id-fast-image1-protocols-autostackprofiles.png (accessed Feb. 07, 2023).
[33] “Decrease sample rate by integer factor - MATLAB downsample - MathWorks Nordic.” https://se.mathworks.com/help/signal/ref/downsample.html?searchHighlight=downsample&s_tid=srchtitle_downsample_1 (accessed June. 01, 2023).
[34] A. Efrat, Q. Fan, and S. Venkatasubramanian, “Curve Matching, Time Warping, and Light Fields: New Algorithms for Computing Similarity between Curves,” *Journal of Mathematical Imaging and Vision*, vol. 27, no. 3, pp. 203–216, Apr. 2007, doi: 10.1007/s10851-006-0647-0.

[35] Wolfram Research, Inc., “Cross-Correlation -- from Wolfram MathWorld.” https://mathworld.wolfram.com/Cross-Correlation.html (accessed June. 01, 2023).
[36] “Align Signals Using Cross-Correlation - MATLAB & Simulink - MathWorks Nordic.” https://se.mathworks.com/help/signal/ug/align-signals-using-cross-correlation.html (accessed June. 01, 2023).
[37] Q. Gong, S. Midlam-Mohler, V. Marano, and G. Rizzoni, “An Iterative Markov Chain Approach for Generating Vehicle Driving Cycles,” *SAE International Journal of Engines*, vol. 4, no. 1, pp. 1035–1045, Apr. 2011, doi: 10.4271/2011-01-0880.
[38] Y.-H. Peng, Y. Zhuang, and Y. Yang, “A driving cycle construction methodology combining *k*-means clustering and Markov model for urban mixed roads,” *Proceedings of the Institution of Mechanical Engineers, Part D: Journal of Automobile Engineering*, vol. 234, no. 2–3, pp. 714–724, Feb. 2020, doi: 10.1177/0954407019848873.
[39] N. Dembski, G. Rizzoni, A. M. Soliman, J. Fravert, and K. Kelly, *Development of Refuse Vehicle Driving and Duty Cycles*. 2005. doi: 10.4271/2005-01-1165.
[40] A. Fotouhi and M. Montazeri-Gh, “Tehran driving cycle development using the k-means clustering method,” *Scientia Iranica*, vol. 20, no. 2, pp. 286–293, Apr. 2013, doi: 10.1016/j.scient.2013.04.001.
[41] “k-means clustering - MATLAB kmeans - MathWorks Nordic.” https://se.mathworks.com/help/stats/kmeans.html#bues3lh (accessed June. 01, 2023).
[42] S. Lloyd, “Least squares quantization in PCM,” *IEEE Transactions on Information Theory*, vol. 28, no. 2, pp. 129–137, Mar. 1982, doi: 10.1109/tit.1982.1056489.
[43] “Smooth noisy data - MATLAB smoothdata - MathWorks Nordic.” https://se.mathworks.com/help/matlab/ref/smoothdata.html (accessed June. 01, 2023).
[44] R. Petrone, D. Hissel, M. Péra, D. Chamagne, and R. Gouriveau, “Accelerated stress test procedures for PEM fuel cells under actual load constraints: State-of-art and proposals,” *International Journal of Hydrogen Energy*, vol. 40, no. 36, pp. 12489–12505, Sep. 2015, doi: 10.1016/j.ijhydene.2015.07.026.

Appendix A1.

This section shows some examples of the vehicle mass data. In these figures are both truck speed [km/h] and weight [tonnes] shown. They are presented here to illustrate how they were of no use in this work. The truck weight seems to increase and decrease in weight by about 1 tonnes, when the truck is driving and it can fluctuate, making the data uninterpretable. This most likely an artefact of the sensors.

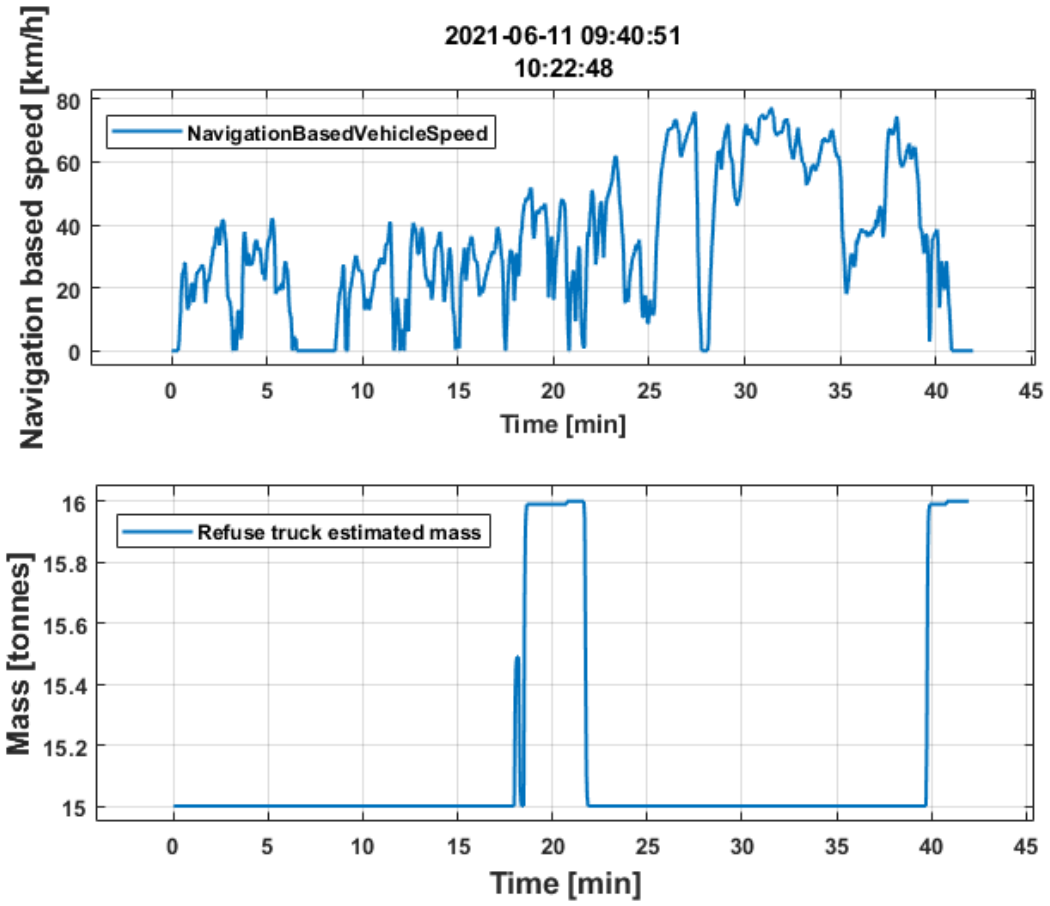

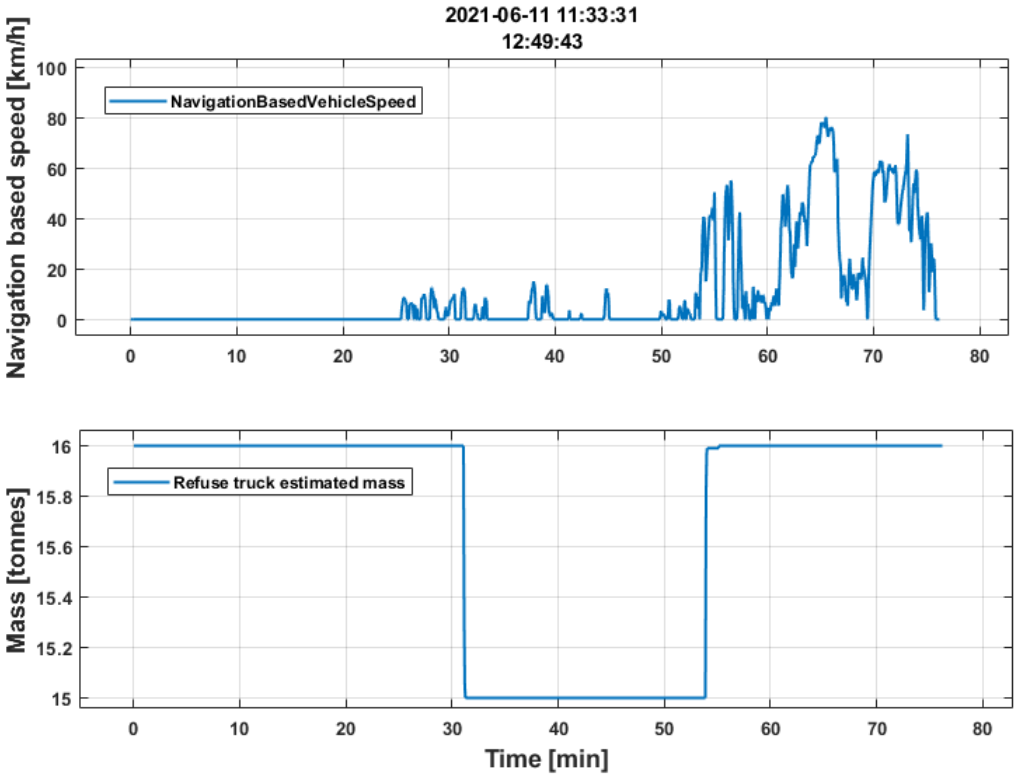
2021-06-11 11:33:31
12:49:43
Navigation based speed [km/h]
NavigationBasedVehicleSpeed
Mass [tonnes]
Refuse truck estimated mass
Time [min]

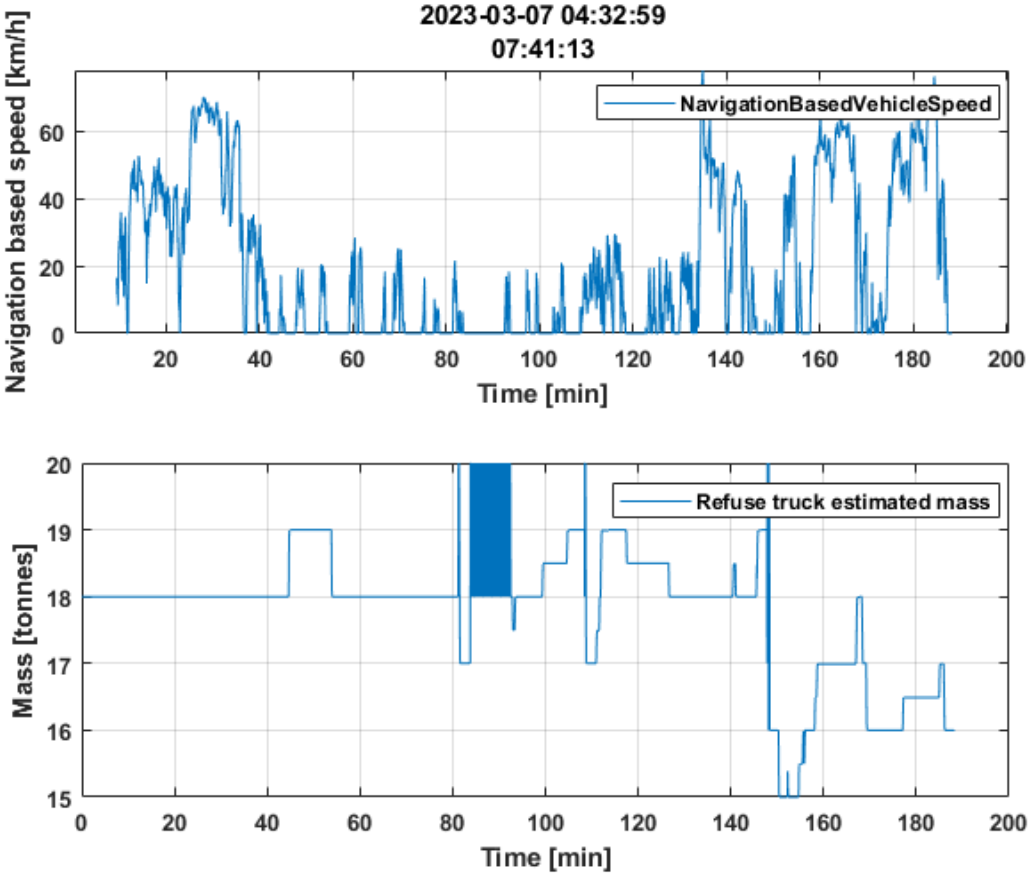
2023-03-07 04:32:59
07:41:13
Navigation based speed [km/h]
NavigationBasedVehicleSpeed
Time [min]
Mass [tonnes]
Refuse truck estimated mass
Time [min]

Appendix A2.

This section will present some of the results from the filtration. The FC power cycles here correspond to fuel cell testing.

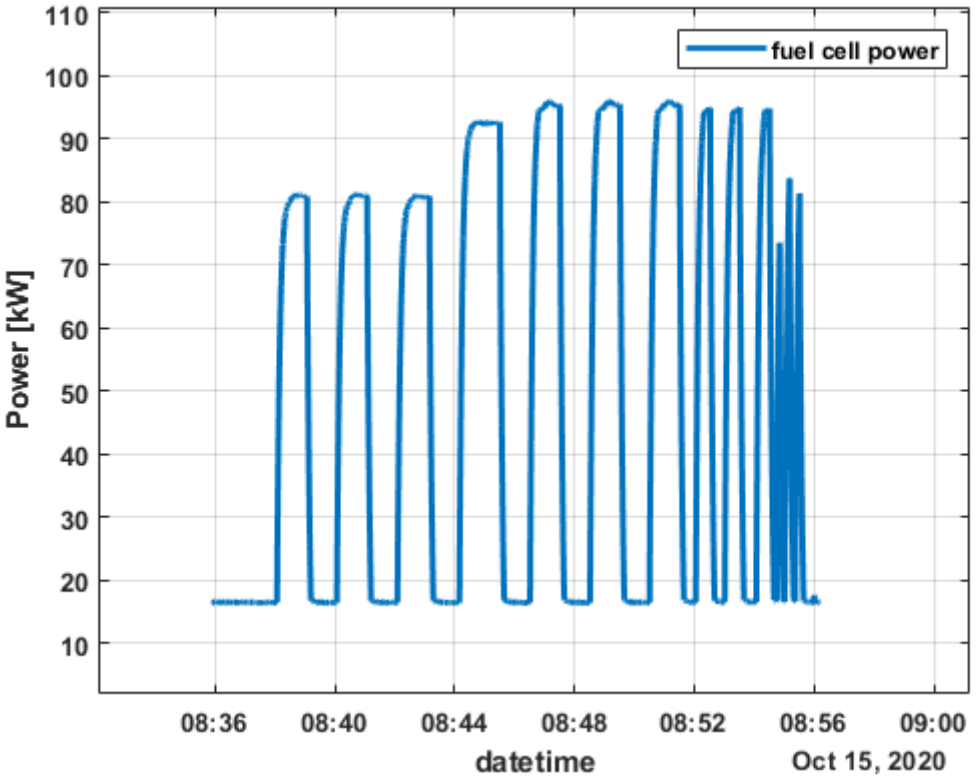

Fuel cell testing

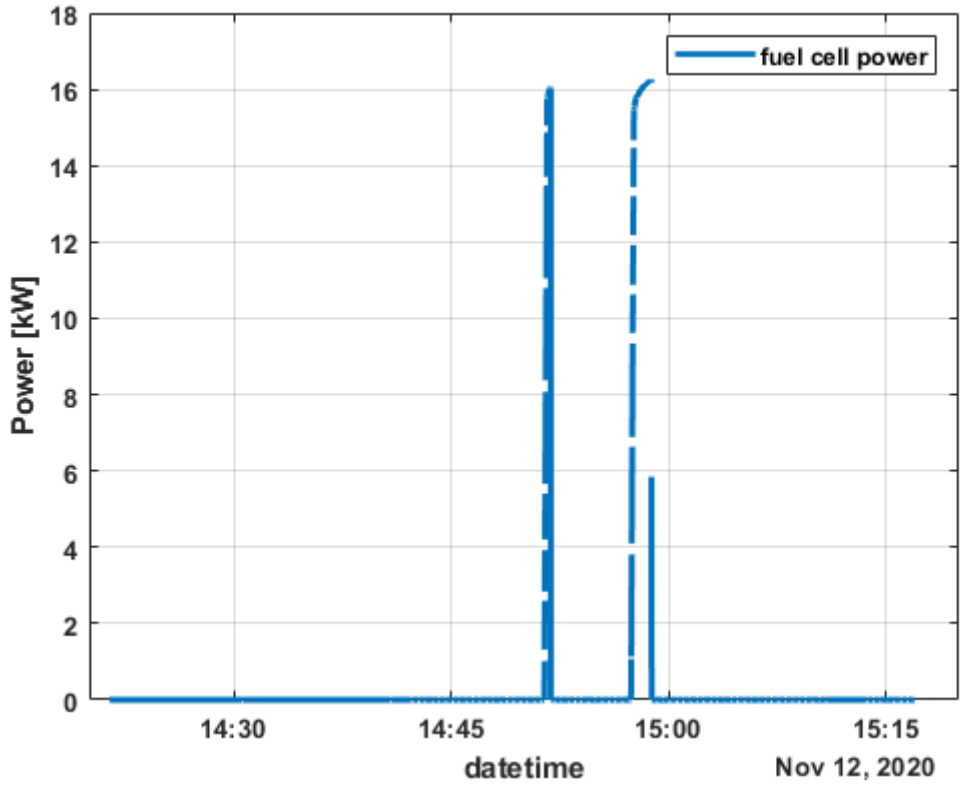

Fuel cell testing

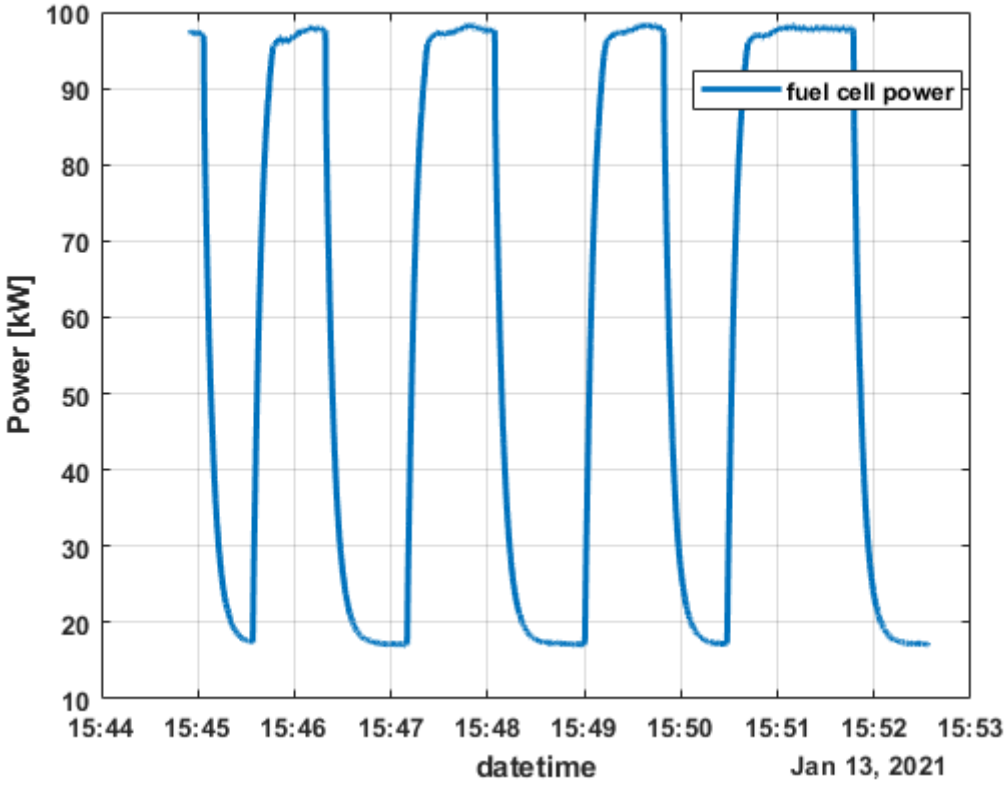

Fuel cell testing

Appendix A3.

Some additional examples of synchronisation results.

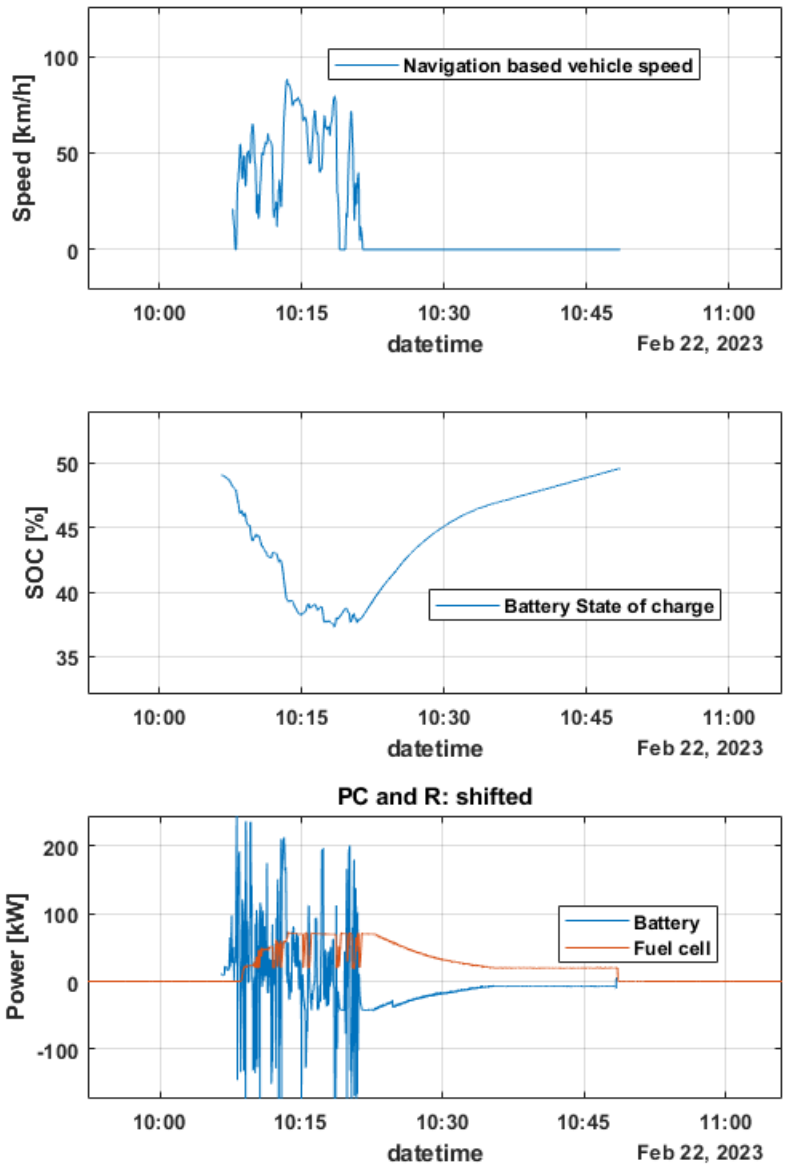

The truck is driving between 10:07 and 10:22. During that time the battery SOC decreases, although it is slowed down by the FC power that is charging the battery. The FC behaves dynamically. After 10:22, the truck is standing still and the FC is transitioning from dynamic to steady state power delivery. Steady state is reached at about 10:35.

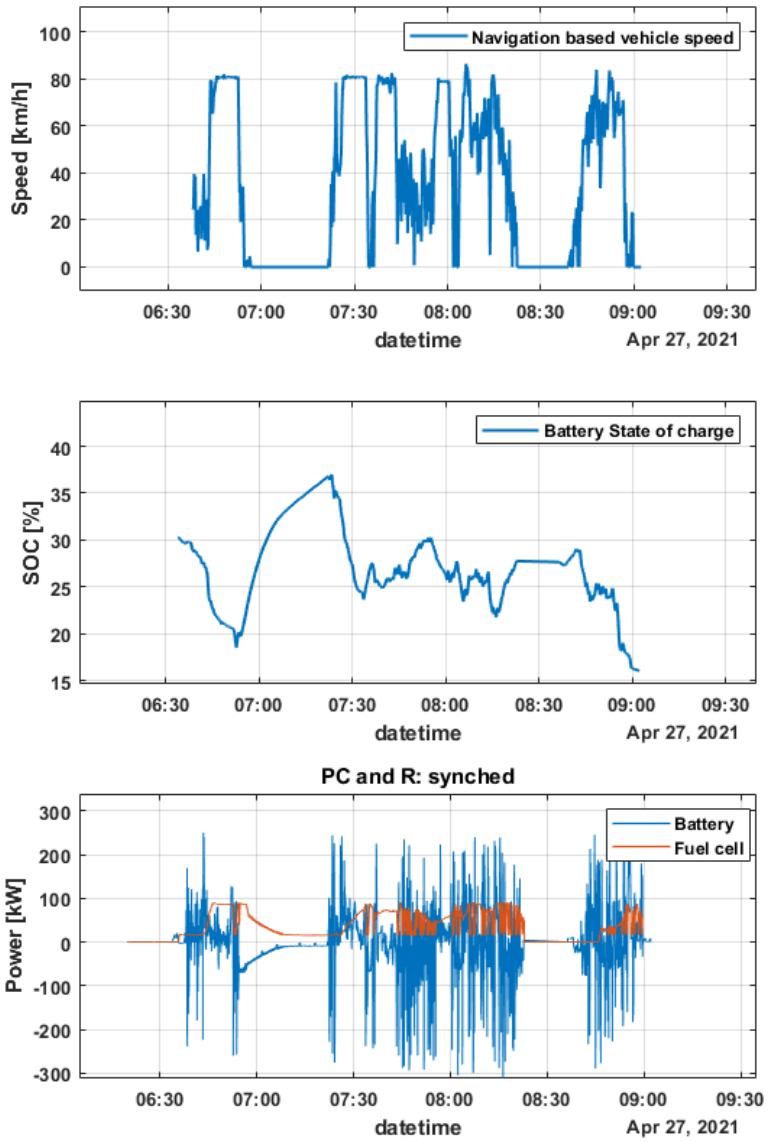

This is one of the more interpretable results from the synchronisation. The truck is driving at high speeds with short breaks between the drive times. From 06:50, the truck is slowing down. The SOC is increasing from 19 to 37 % during the break that stops at 07:25. The FC is charging the battery with a dynamic and steady state power profile. After the break the truck drives at high speeds again. A low medium speed segment can be seen around 07:45 which then transitions to high speed again. Between 07:30 to about 08:45 the SOC is shifting between 25 and 30 %. The FC behaves dynamically at high power (70 kW). This example consisted of one FC file and two S-set (battery) files.

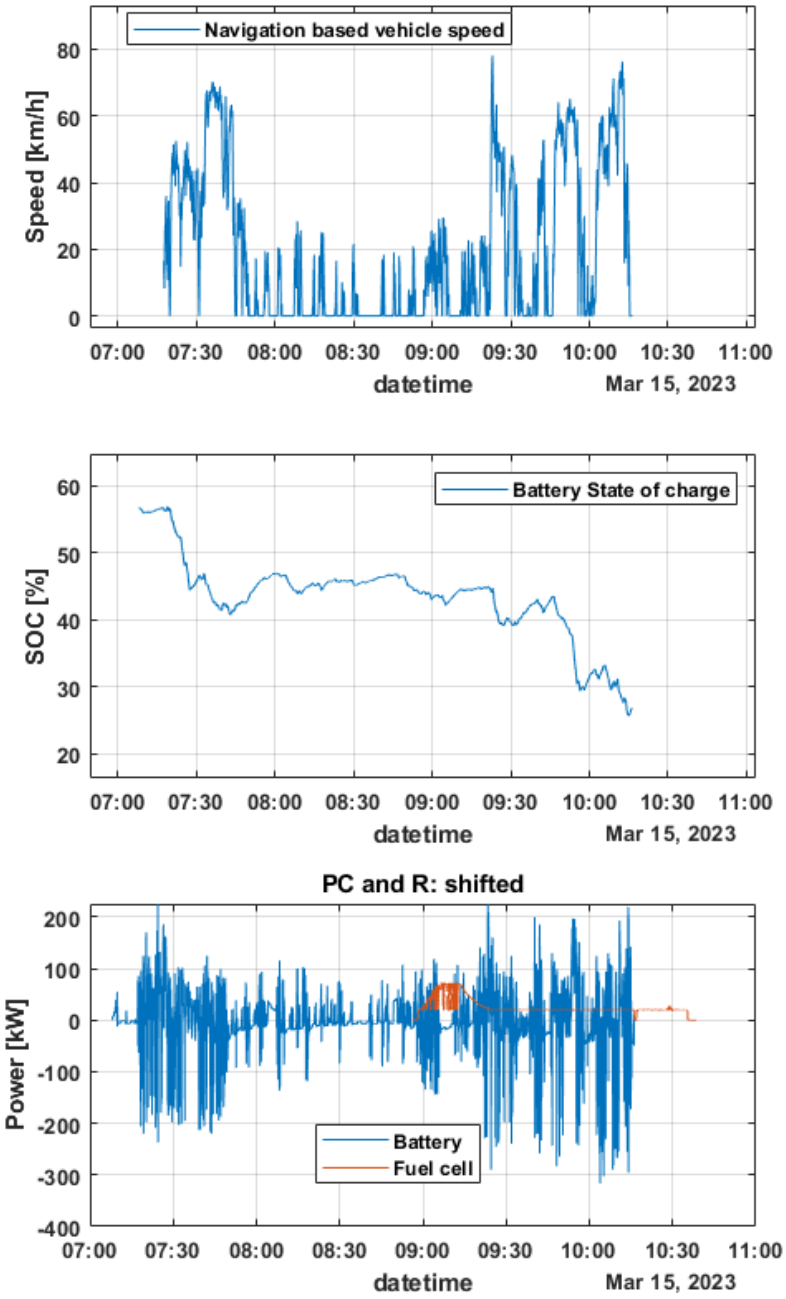

This is one of the less interpretable results from the synchronisation. The battery data here comes from one file and FC data from one file. The truck is seen to drive at both high and low speeds. The SOC is seen to decrease, although it fluctuates between 40 and 50 % until it finally decreases once the truck reaches high speeds at 09:25. The FC power profiles consist of both dynamic and steady state segments. In this case the battery time should probably be shifted so it ends where the FC power reaches 0 kW at the end of the time data.

Appendix A4.

More examples of categorised micro trips. The micro-trips can be characterised by the level of power request. For example, the standing still micro-trips shown in this report (e.g. 4.1) are almost always a short time of steady state power delivery at 20 kW. However, some, but a few, files display a different profile in the standing still category. This example can be seen in this Appendix A4. It is showing a more dynamic behaviour as it is decreasing power requests from 40 to 30 kW in a 4 minute time span. Iconic for urban and non-urban is that they can consist of FC power profiles of both steady state and dynamic behaviour. Difference is the time duration and power level. Non-urban lasts longer and requires more power since it does longer driving trips at higher speeds, hence more power is required. Although, what is noteworthy is that the dynamic behaviour seems to jump between 20 kW and 60 or 80 kW (if urban or non-urban).

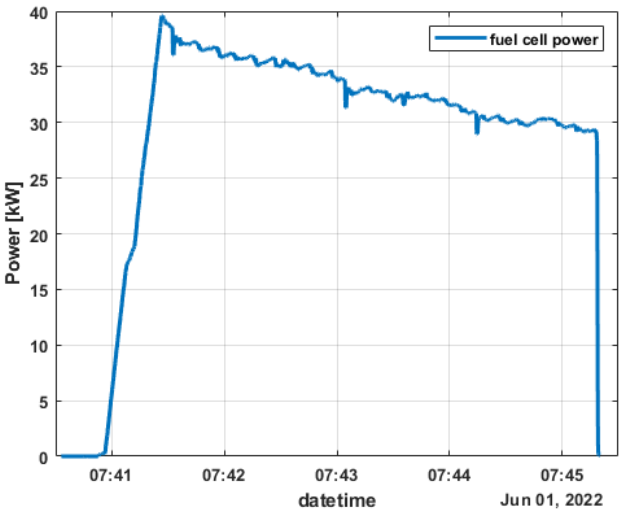

Standing still (charging)

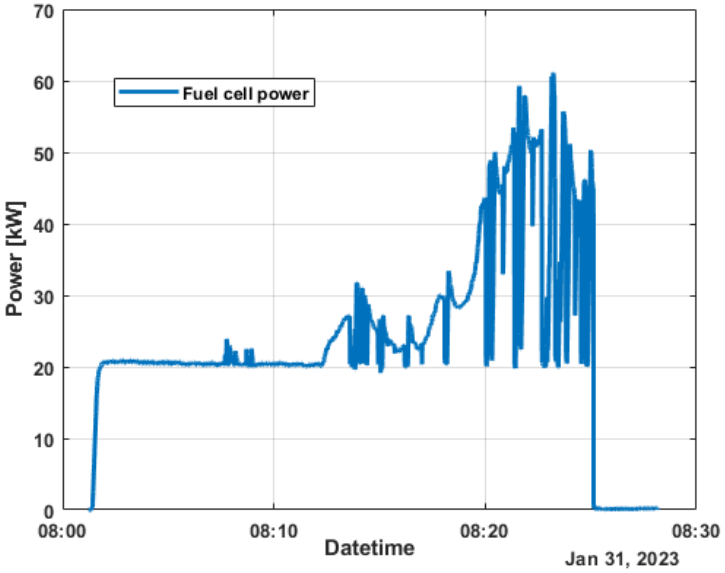

Urban driving

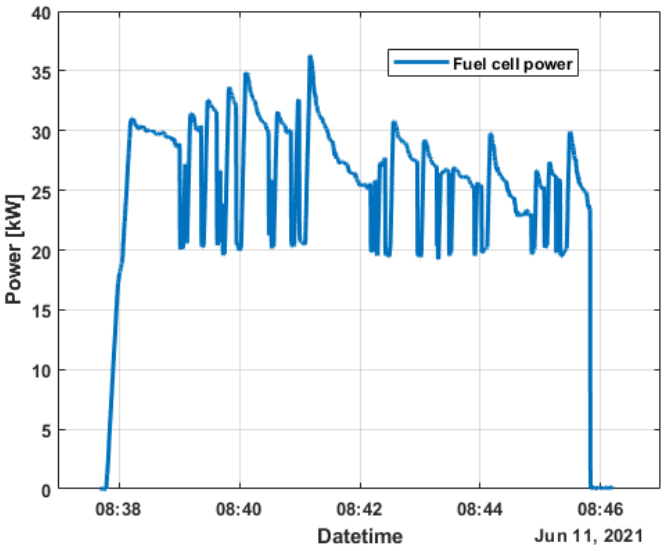

Urban driving

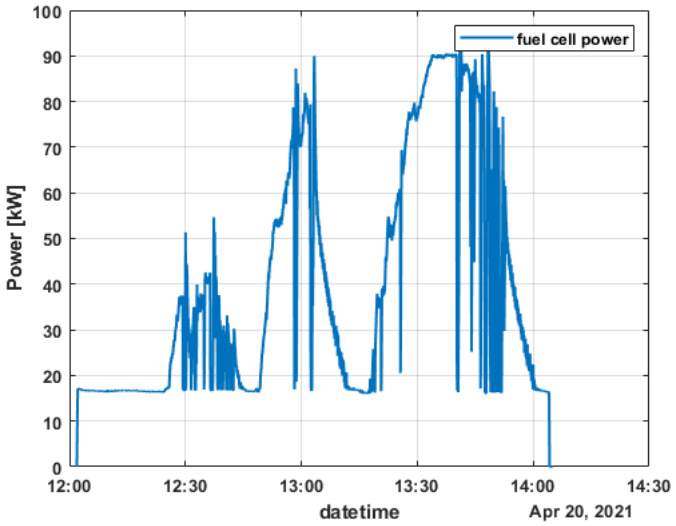

Non-urban

In the example above, it consists of both charging, urban and non-urban. It is labelled non-urban since it comprehends the majority of the power profile.

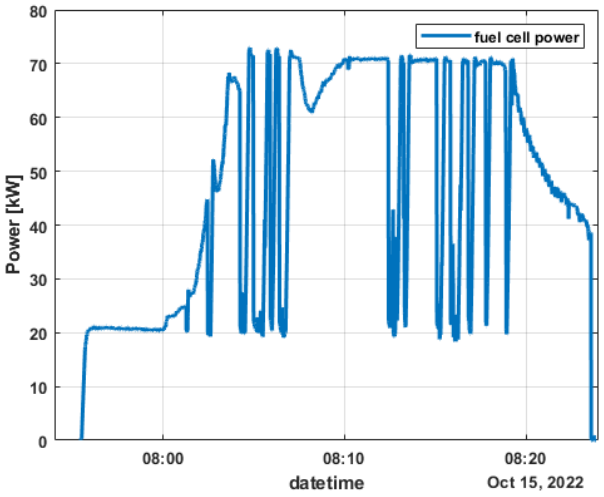

Non-urban